Simulation of Arctic Diamond Dust, Ice Fog, and Thin Stratus Using an Explicit Aerosol–Cloud–Radiation Model

ERIC GIRARD

Department of Aerospace Engineering Sciences, University of Colorado, Boulder, Colorado

JEAN-PIERRE BLANCHET

Département des Sciences de la Terre et de l'Atmosphère, Université du Québec à Montréal, Montreal, Quebec, Canada

(Manuscript received 12 July 1999, in final form 8 June 2000)

ABSTRACT

In support to the development of the Northern Aerosol Regional Climate Model, a single column model with explicit aerosol and cloud microphysics is described. It is designed specifically to investigate cloud–aerosol interactions in the Arctic. A total of 38 size bins discretize the aerosol and cloud spectra from 0.01- to 500-μm diameter. The model is based on three equations describing the time evolution of the aerosol, cloud droplet, and ice crystal spectra. The following physical processes are simulated: coagulation, sedimentation, nucleation, coalescence, aggregation, condensation, and deposition. Further, the model accounts for the water–ice phase interaction through the homogeneous and heterogeneous freezing, ice nuclei, and the Bergeron effect. The model has been validated against observations and other models.

In this paper, the model is used to simulate diamond dust and ice fog in the Arctic during winter. It is shown that simulated cloud features such as cloud phase, cloud particle diameter, number concentration, and mass concentration are in agreement with observations. The observed vertical structure of mixed-phase cloud is also reproduced with the maximum mass of liquid phase in the upper part of the cloud. Based on simulations, a hypothesis is formulated to explain the thermodynamical unstable mixed-phase state that can last several days in diamond dust events. The ice supersaturation time evolution is assessed and is compared to its evolution in cirrus clouds. It is shown that the supersaturation relaxation time, defined as the time required for supersaturation to decrease by a factor e, is more than 10 times the value found in cirrus clouds. Finally, the radiative contribution of arctic diamond dust and ice fog to the downward longwave radiation flux at the surface is evaluated and compared to observations.

1. Introduction

Clouds play an important role in climate regulation by absorbing and scattering solar and terrestrial radiation. In the Arctic, the role and effect of clouds on climate are more complex due to the highly reflecting snow–ice surface, the low temperature, and amount of water vapor and the surface-based temperature inversion (Curry et al. 1996). Although many efforts have been devoted to cloud studies on a global basis, very few have focused on arctic clouds. Further, even the physical processes controlling the formation and evolution of arctic clouds are not well understood (Curry et al. 1996).

Despite strong surface inversion and extremely stable atmosphere during winter, low stable clouds are very common in the Arctic. Observations show high frequencies of diamond dust events and ice fog (Maxwell 1982; Curry et al. 1990; Girard 1998). Despite the very cold temperatures of the lower troposphere, mixed-phase stratus clouds and diamond dust have been observed with a frequency of about 30% during the Surface Heat Budget of the Arctic Ocean (SHEBA) experiment over the Beaufort Sea during winter 1998 (Curry et al. 2000). Other cases of observed mixed-phase clouds during the cold half of the year have been reported during previous experiments (Witte 1968; Pinto 1998). Although generally optically thin, these clouds contribute a significative amount to the downward longwave radiative flux to the surface (Witte 1968; Curry et al. 1996).

Autumn and spring are characterized by a very high frequency of mixed-phase clouds (Curry et al. 1990; Curry and Radke 1993). Autumn marks the transition from almost exclusively liquid phase boundary layer clouds during summer to predominantly crystalline win-

Corresponding author address: Eric Girard, Department of Aerospace Engineering Sciences, CB 429, University of Colorado, Boulder, CO 80309-0429.
E-mail: girard@cires.colorado.edu

ter clouds. Observations show that cloud phase does not depend only on the temperature. Indeed, ice crystals have been observed at temperature up to −4°C while supercooled water droplets can stay in liquid phase at temperature as low as −30°C (Witte 1968; Curry et al. 1996). Some laboratory experiments (Pruppacher and Klett 1997) as well as measurements in the Arctic (Pinto 1998; Rangno and Hobbs 2001) suggest that the mean water droplet size is an important factor determining whether or not a cloud will glaciate. Also, Borys (1989) has shown that the aerosol composition seems to play a major role in the ice deposition nuclei efficiency.

Several radiative feedbacks occurring in the Arctic involving clouds have been identified so far (Curry et al. 1996). Many feedbacks involve the cloud–aerosol interactions. Aerosols are closely linked to clouds since some of them can act as condensation nuclei (CN) or ice nuclei (IN). The cloud-drop size feedback, the water content feedback, and the cloud phase and precipitation feedbacks might be substantial contributors to the arctic climate [see Curry et al. (1996) for a comprehensive review]. For example, Blanchet and Girard (1994, 1995) have hypothesized that the anthropogenic sulfuric aerosols, present in large concentration during the arctic winter, alter the ice forming properties of the aerosol and reduce the ice crystal number concentration, increase their size, and enhance the dehydration rate of the lower troposphere leading to a surface cooling. This feedback, known as the dehydration-greenhouse feedback, is one among many others that need to be investigated in more detail. To improve our understanding of aerosol–cloud interactions in the Arctic and to develop parameterizations of these processes for global models, comprehensive models and extensive measurements are necessary.

The objective of the Northern Aerosol Regional Climate Model (NARCM) is to simulate the direct and indirect effects of aerosol on the northern latitude climate. In that context, to address cloud–aerosol interactions in the Arctic, we have developed a comprehensive radiation-aerosol-cloud model able to simulate the aerosol dynamics and the formation and evolution of diamond dusts, arctic fog, and thin stratus. This model covers the entire range of particle sizes, from the Aitken aerosol particles at 0.01 μm to the ice crystals and water droplets with diameter of the order of 100 μm. Many models have been developed for the simulation of cirrus clouds and boundary layer ice clouds (Starr and Cox 1985; Mitchell 1994; Khvorostyanov and Sassen 1998a,b). However, in these models, either the cloud spectrum or the aerosol spectrum is prescribed. The model described in this paper differs from the others in that it explicitly simulates both aerosol and cloud particles and their interactions.

This model can be used to investigate and eventually parameterize cloud formation and time evolution as well as specific processes relating aerosols and clouds. For instance, it has been used to parameterize diamond dust and ice fog in the Arctic during winter (Girard and Blanchet 2001). It can also be used more generally as a tool to develop new parameterizations of different aspects of the aerosol–cloud processes believed to alter the climate through indirect aerosol radiative effects. In this paper, we use this model to investigate diamond dust and ice fog formation during winter in a context of an infrared radiative cooling of a maritime arctic air mass.

2. The model

The model is used to simulate clouds in which turbulence and entrainment are weak such as in the low-level ice crystal precipitation and ice fog occurring during winter over the Arctic. It can also be used to simulate thin stratus or thin cirrus at high altitude. This model has been developed to focus preliminarily on the aerosol–cloud interactions acting to form ice crystals and water droplets in a context of very stable air mass, such as those observed in the Arctic during winter. The general structure of the model is similar to the column model of Curry (1983). It has two main parts: 1) a longwave radiation scheme and 2) a microphysics scheme.

The radiation schemes are those used in the GCM of the Canadian Climate Center (McFarlane et al. 1992). The model has six spectral bands in the infrared spectrum. Cloud emissivity is parameterized as function of the equivalent radius and the optical water path following Platt and Harshvardhan (1988). The optical water path is provided by the explicit microphysics scheme described below. The cloud albedo is calculated with the Delta–Eddington method (Joseph et al. 1976). The following gases are accounted for: water vapor, carbon dioxide, CFCs, ozone, and methane.

The microphysics part of the model is based on MAEROS2, an aerosol dynamics model developed by Gelbard et al. (1980). MAEROS2 computes the time evolution of size-segregated particles in the atmosphere including condensed water. The scheme has been included into the multilayer atmospheric model. Only one phase, liquid or solid, is allowed in a size bin. This allows the number of prognostic variables and the cost of the model to be reduced. Modifications to MAEROS2 have been made to account for Kelvin and solution effects on diffusional growth of the haze droplets. In our version of MAEROS2, three constituents are considered: water vapor, aerosols, and condensate (ice crystals or water droplets). The five basic equations in the model are

$$\frac{\partial}{\partial t}m_A(r) = K\frac{\partial^2}{\partial z^2}m_A(r) + S_{A_{\text{cond}}} + S_{A_{\text{depo}}} + S_{A_{\text{coag}}} + S_{A_{\text{sedi}}} + S_{A_{\text{nucl}}}, \quad (1)$$

$$\frac{\partial}{\partial t}m_I(r) = K\frac{\partial^2}{\partial z^2}m_I(r) + S_{I_{\text{depo}}} + S_{I_{\text{aggr}}} + S_{I_{\text{sedi}}} + S_{I_{\text{nucl}}} + S_{I_{\text{phas}}}, \quad (2)$$

$$\frac{\partial}{\partial t}m_W(r) = K\frac{\partial^2}{\partial z^2}m_W(r) + S_{W_{\text{cond}}} + S_{W_{\text{coal}}} + S_{W_{\text{sedi}}} + S_{W_{\text{nucl}}} + S_{W_{\text{phas}}}, \quad (3)$$

$$\frac{\partial q}{\partial t} = K\frac{\partial^2 q}{\partial z^2} + S_{I_{\text{depo}}} + S_{W_{\text{cond}}} + S_{A_{\text{cond}}} + S_{A_{\text{depo}}}, \quad (4)$$

$$\frac{\partial T}{\partial t} = K\frac{\partial^2 T}{\partial z^2} + \frac{Q_{\text{rad}}}{C_p} + \frac{Q_{\text{cond}}}{C_p} + \frac{Q_{\text{depo}}}{C_p}, \quad (5)$$

$$\frac{d\delta}{dt} = -\left(\frac{L_v}{R_v T^2}\right)\frac{\partial T}{\partial t} - \left(\frac{p}{\varepsilon e_s}\right) \times [S_{W_{\text{cond}}} + S_{I_{\text{depo}}} + S_{A_{\text{cond}}} + S_{A_{\text{depo}}}], \quad (6)$$

where the first three equations describe the time evolution of the mass of aerosols (m_A), ice crystals (m_I), and water droplets (m_W). Besides the microphysics equations, there is an equation for specific humidity (q), temperature (T), and saturation ratio (δ). Only the partial time derivative is considered in the model since the vertical and horizontal advections are neglected. Anticyclonic conditions generally prevailing in diamond dust and ice fog events may favor a small subsidence varying between 0 and 0.5 cm s^{-1}. However, Curry (1983) has shown that the main effect of the subsidence is to warm the top of the saturated layer and delay the upward propagation of the airmass cooling. Due to the high cost of this model, we choose to neglect this process allowing a quicker cloud formation. Horizontal concentrations of ice crystals, water droplets, and aerosols are assumed constant and the vertical transport is allowed only by gravitational sedimentation. The first term on the right-hand side of Eqs. (1)–(5) is an eddy diffusion term. The eddy diffusivity coefficient K is set to 0.1 m^2 s^{-1}, which is representative of a stable environment. The terms S_x represent several microphysical processes acting either as a source or a sink: condensation (cond), deposition (depo), coagulation (coag), sedimentation (sedi), and nucleation (nucl) for aerosols; deposition, aggregation (aggr), sedimentation, nucleation, and phase change (phas) for ice crystals; condensation, coalescence, sedimentation, nucleation, and phase change for water droplets. Terms related to aerosols are described in Gelbard et al. (1980). Source terms related to ice crystals and water droplets are described in this section. The humidity depends on the total mass variations of the ice crystal and water droplets. Therefore, it varies according to the deposition of water onto ice crystals and aerosols, and the condensation of water vapor onto water droplets and aerosols. The saturation equation [Eq. (6)] is a balance between two terms. The first one is the rate of production of available water vapor to condensate. In the case studied in this work, it is proportional to the infrared radiative air cooling rate since no vertical or horizontal advection is considered. The second term represents the rate of condensation onto aerosols, water droplets, and ice crystals. Finally, the temperature is a function of the radiation balance and the latent heat release of fusion and sublimation.

TABLE 1. Discrete size bins used in MAEROS2 to represent aerosol and cloud size distributions.

Size bin	Diameter (μm)	Size bin	Diameter (μm)
1	0.010–0.013	20	2.236–2.973
2	0.013–0.017	21	2.973–3.952
3	0.017–0.023	22	3.952–5.254
4	0.023–0.031	23	5.254–6.984
5	0.031–0.041	24	6.984–9.285
6	0.041–0.055	25	9.285–12.34
7	0.055–0.073	26	12.34–16.41
8	0.073–0.098	27	16.41–21.81
9	0.098–0.130	28	21.81–29.00
10	0.130–0.172	29	29.00–38.55
11	0.172–0.229	30	38.55–51.25
12	0.229–0.305	31	51.25–68.14
13	0.305–0.405	32	68.14–90.58
14	0.405–0.539	33	90.58–120.4
15	0.539–0.716	34	120.4–160.1
16	0.716–0.952	35	160.1–212.8
17	0.952–1.265	36	212.8–282.9
18	1.265–1.682	37	282.9–376.1
19	1.682–2.236	38	376.1–500.0

This system of six equations is integrated numerically for each atmospheric layer. A Runge–Kutta numerical method is used with a self adaptable time step. Time step is smaller than 1 s and can be as small as 0.1 s to resolve condensation and deposition.

Table 1 shows the 38 size bins used in the model. A numerical constraint of MAEROS2 imposes a size grid decreasing with diameter by a factor two between successive size ranges. As a result, the size resolution is about 0.01 μm for CN whereas larger particles like cloud droplets and ice crystals have lower resolution. This procedure allows six orders of magnitude of particulate sizes to be treated simultaneously. Also this constraint allows significant simplifications of the calculation of the coagulation process (Gelbard et al. 1980).

Equations (1) and (2) or (1) and (3) (depending on the water phase present in a given size bin) are integrated for each size bin. The mass transfer between each size bin is done through coagulation, condensation, coalescence, aggregation, and deposition. In application, the model can simulate the evolution of the aerosol spectrum, the formation of CN and the activation and evolution of the water droplets and ice crystals. Thus, it covers the entire spectrum from Aitken particles to diamond dust of the order of 100 μm in size. Physical processes involved in the formation of large rain droplets, large snowflakes, or hail are not accounted for since they are not relevant for the arctic thin boundary layer clouds.

a. Ice crystal characteristics

Ice crystal habits are varied and traditionally have been thought to depend on temperature and humidity (Pruppacher and Klett 1997). However, more recent studies have shown that no simple relationship exists between the crystal habit and the ambient conditions. Meyers and Hallet (1998) have observed a higher frequency of occurrence of column habit when the sulfur concentration is higher, thus, suggesting that aerosol composition may play a role. Laboratory experiments of Bailey and Hallet (1998) indicate that column-needle shape ice crystals are more likely to form at water supersaturation and very low temperature.

Few observations of ice crystal have been made in the lower troposphere in the Arctic during winter. Existing observations suggest that various ice crystal habit such as plates, column, or mixed and irregular can coexist in the same ambient air (Hoff 1988; Hoff and Leaitch 1989; Curry et al. 2000). However, conditions of ambient air in these observations are not necessarily an indication of the conditions prevailing during the ice crystal formation, which may have occurred higher in the atmosphere.

Given the conditions of very cold temperature and high concentration of sulfuric acid (Barrie 1986), which prevail in the Arctic during winter, we assume a column shape with a length-axial radius ratio of 10. This ratio is based on the observations that Ohtake et al. (1982) made in Barrow, Alaska. In the model, ice crystal size is given by the equivalent diameter, which is defined as the diameter corresponding to a spherical ice crystal of the same mass. The density varies with the ice crystal dimension as described in Heymsfield (1972).

b. The collision processes

Three collision processes are allowed for in the model: aerosol coagulation, cloud droplet coalescence, and ice crystal aggregation. The explicit collision scheme of Gelbard et al. (1980), based on the stochastic collection equation, is used. The collection efficiency is the probability that two drops collide and stick together and is the product of the probability of collision, the collision efficiency, and the probability of sticking or the coalescence efficiency. While the collision efficiency is calculated explicitly following the method based on particle mass of Gelbard et al. (1980), the coalescence efficiency is fixed for each kind of collision. Collisions between cloud droplets and aerosols, and between ice crystals and aerosols, are not accounted for. The large discrepancy between sizes of cloud particles and aerosols make the collision efficiency very low. Consequently, it is reasonable to neglect this process for short simulations of few days.

Very few quantitative measurements on sticking efficiency of aerosols are available. According to Pruppacher and Klett (1997), the fact that the kinetic energy involved in this kind of collision is very small makes rebound unlikely. We have then assumed a sticking efficiency of unity.

Laboratory experiments have shown that cloud water droplets of sizes less than 1 μm have a coalescence factor of unity, meaning that each time they collide they stick together (Pruppacher and Klett 1997; Hu et al. 1998). For cloud droplets of larger sizes, the sticking factor is less than unity and can be as low as 0.1. This arises from the drop deformation during its fall out and the high ratio between the collision energy and the surface energy (Hu et al. 1998). Since in the Arctic during autumn, winter, and spring, the liquid water droplets are typically smaller than 100 μm in diameter (Witte 1968; Pinto 1998; Curry et al. 2000), we assume in the model a coalescence factor of 1.

For ice crystal aggregation, it appears that the sticking factor is a strong function of temperature, humidity, and crystal habit. It may vary between 0.1 and 0.5 (Pruppacher and Klett 1997). In the model, the sticking factor for ice crystal aggregation is fixed at 0.3. This value is representative of the aggregation efficiency obtained during laboratory experiments involving collisions between planar crystals in the temperature range -20 to -30°C (Mitchell 1988).

Riming, or collision between water droplets and ice crystals, is not considered. To avoid numerical instability, density of particles that collide must not differ by more than a factor 2. Therefore, simulation of riming is impossible with this model in this configuration. However, the error introduced by this approximation is limited by the fact that 1) the particle concentration in diamond dust event is very low, and 2) the riming probability is low, with a maximum of 30% for a very limited size range of ice crystals and water droplets (Pruppacher and Klett 1997). These two factors contribute to minimize significantly the riming rate in diamond dust. Consequently, although this approximation is expected to slightly underestimate the mean cloud particle diameter, large errors resulting from this approximation are not expected for the reasons cited above.

c. Water condensation and ice deposition

In the model, the condensation rate and the deposition rate are calculated as follows:

$$S_{J_{\text{cond}}} = 4\pi r D\left[\rho - \rho_{sw}\left(1 + \frac{a}{r} - \beta\frac{b}{r^3}\right)\right]K_c, \quad (7)$$

$$S_{J_{\text{depo}}} = 4\pi C D\left[\rho - \rho_{si}\left(1 + \frac{a}{r} - \beta\frac{b}{r^3}\right)\right]K_c, \quad (8)$$

where r is the water droplet or ice crystal radius; ρ is the water vapor density; ρ_{sw} and ρ_{si} are the water vapor density at water and ice saturation, respectively; D is the molecular diffusion coefficient; and the indice J represents either CN and water droplets in Eq. (7) or IN

and ice crystals in Eq. (8). Here K_c is a nondimensional factor accounting for the kinetic behavior of aerosols smaller than 0.1 μm and is calculated using the parameterization of Fuch and Sutugin (1971). The capacitance C is a factor that accounts for the nonspherical shape of ice crystals. According to Rogers and Yau (1989), the capacitance of a column shape crystal can be approximated by the capacitance of a prolate spheroid of major and minor axis k and l; that is,

$$C = \frac{\sqrt{k^2 + l^2}}{\ln\left[\frac{k + \sqrt{k^2 + l^2}}{l}\right]}. \quad (9)$$

In the condensation process, the curvature and solution effects must be considered to determine the equilibrium size of haze particles. Also, the reduction of water vapor saturation pressure near small solution particles is essential to determine the critical supersaturation that onsets activation. For nuclei larger than or equal to 0.1 μm, the curvature effect and solution effect can be approximated by the terms a/r and $\beta b/r^3$, respectively, in Eqs. (7) and (8) (Rogers and Yau 1989). The parameter a depends on temperature and b varies with the solute mass in the solution and the Van Hoff factor, which depends on the solute nature. The parameter β represents the volume soluble fraction of the particles. Note that both β and b are determined by the aerosol solute composition, which is set initially for each simulation. Therefore, by setting these parameters with the appropriate value, the model allows for internally mixed aerosols with different proportion of soluble materials.

d. Sedimentation

For gravitational sedimentation of water droplets, we assume that the terminal velocity of small spherical particles is described by the Stokes regime if they are smaller than 40 μm, that is proportional to the square of the particle radius, $V_W = K_1 r^2$, with $K_1 = 1.19 \times 10^6$ cm^{-1} s^{-1}. For particles larger than 40 μm, the viscous drag is considered and the ice crystal terminal velocity (V_I) is proportional to the particle radius (e.g., Pruppacher and Klett 1997), $V_W = K_2 r$ with $K_2 = 8 \times 10^3$ s^{-1}.

The terminal velocity of an ice crystal strongly depends on its habit. The ice crystal shape determines its density and its drag force to the flow when falling. Following the method used by Gelbard et al. (1980), we correct the terminal velocity with the shape factor f as follows:

$$V_I = \frac{V_W}{f}, \quad (10)$$

where f is greater than unity and V_W is the terminal velocity of a water droplet having the same volume. The shape factor is defined as the ratio of the drag force associated to the crystal over the drag force of a sphere of equivalent mass going at the same velocity. Assuming a Reynolds number of 1, then the shape factor f can be expressed as follows:

$$f = 0.0005 \frac{\rho_I}{r_{\text{sphere}}} L_I, \quad (11)$$

where L_I and r_I are, respectively, the length and density of the columnar crystal and r_{sphere} is the radius of a sphere of an equivalent mass to the columnar crystal. The r_{sphere} can be easily calculated knowing that the length-axial radius ratio of the ice crystal is 10. The ice crystal density is determined using the parameterization of Heymsfield (1972) for columnar crystals at temperatures below -20°C:

$$\rho_I = 0.65 L_I^{-0.0915}, \quad (12)$$

with the length (in mm) and the density (in g m^{-3}). A uniform distribution of the ice and water mixing ratio within the volume formed by two adjacent layers is assumed. The sedimentation term S_{sedi} in (2) and (3) is then given by the following expression:

$$S_{x_{\text{sedi}}} = \frac{V_x}{\Delta z} m_x, \quad (13)$$

where x stands for ice or liquid and Δz is the height between two levels.

e. Ice crystal nucleation

Processes related to ice crystal nucleation are of key importance since they determine the ice crystal concentration and the ice water mixing ratio. Originally, researchers thought that heterogeneous nucleation was entirely responsible for ice crystals nucleation in the atmosphere. However, observations and modeling have shown that heterogeneous nucleation alone cannot produce observed ice crystal concentrations. According to Curry et al. (1990), the ice forming nucleus concentration in the Arctic is rarely higher than 1 L^{-1} while ice crystal concentration varies between 1 and 1000 L^{-1}. In cirrus clouds, where temperatures are similar to those of the lower arctic troposphere during winter, the same low ratio between IN and ice crystal concentration has been observed (Sassen and Dodd 1988; Heymsfield and Sabin 1989). The SHEBA–First International Satellite Cloud Climatology Project (ISCCP) Regional Experiment (FIRE) experiment has shown that IN concentration is also very low during spring (Rogers et al. 2001). Only few episodes of higher IN concentration of the order of 10 L^{-1} have been observed downstream of open leads. Biogenic sources from the ocean, such as some phytoplankton species, are active at temperature as high as -3°C (Szyrmer and Zawadzki 1997). These biogenic IN are likely to contribute significantly to these high IN episodes near leads. Given the radiative importance of the partitioning of cloud water into liquid and ice in the

simulation of the arctic lower troposphere, we briefly review the current knowledge.

To explain the enhanced ice crystal concentration in pristine environments such as in cirrus or in the Arctic during winter, three processes have been proposed so far: homogeneous freezing of haze droplets (Ohtake 1993; Curry et al. 1996), break up of ice crystals (Pruppacher and Klett 1997; Swanson et al. 1998), and the chemical transformation of aerosol during cloud processing (Rosinski 1991). In the extremely stable lower troposphere of the Arctic, ice crystal breakup by collisions cannot explain ice crystal concentration, since this process requires violent collisions between ice crystals such as those produced by strong vertical velocity and turbulence in convective clouds. Swanson et al. (1998) have suggested another break-up process. They showed in laboratory experiments that ice crystals falling in a subsaturated layer can break up during the sublimation process without any turbulence or convection. This process would be particularly efficient for column-needle crystal shape. Although potentially effective in the Arctic, measurements are needed to quantitatively assess the importance of this process on ice crystal multiplication.

According to Rosinski (1991), ineffective IN that experience many condensation evaporation cycles can be transformed into effective IN by chemical reactions during cloud processing. In laboratory experiments, Rosinski has shown that ammonium sulfate, an excellent CN but poor IN, may be transformed during cloud processing into effective IN by the deposition of insoluble aggregate onto its surface. This ice nucleation process might provide about 0.01–0.1 IN per liter (Rosinski et al. 1995). However, this formation mechanism of IN has not been verified for complex mixtures of aerosols coated with sulfuric acid, which are the dominant aerosols in the arctic troposphere during winter and spring. Other observations are clearly needed to assess the importance of this mechanism in the Arctic.

Many observations in the Arctic report liquid cloud droplets at temperatures as low as −30°C. Witte (1968) observed liquid condensate at temperatures as low as −32°C in December 1967. Jayaweera and Ohtake (1973) observed very few ice crystals above −20°C in September 1971 and April 1972. Ohtake (1993) hypothesized that the main ice nucleation process is the condensation of water vapor on sulfuric acid aerosols followed by the homogeneous freezing when particles are sufficiently diluted. Further, it has been hypothesized that pollution-derived sulfuric acid aerosols, in large concentration during the arctic winter and spring (Barrie 1986), might deactivate IN by coagulating with them (Curry et al. 1996).

Other observations suggest that the ice nucleation occurs at higher temperatures. Curry et al. (1990) report a high frequency of ice crystals at temperatures ranging from −20°C to −8°C. Laboratory experiments (e.g., Pruppacher and Klett 1997) and observations (Curry et al. 2000) have also shown that large water droplets freeze more rapidly than smaller ones. No conclusion can be made based on the small number of observations available; however, it is reasonable to assume that both heterogeneous and homogeneous nucleation may occur in different proportions that vary in time and space.

Both homogeneous and heterogeneous ice nucleation are simulated in the model. For the heterogeneous ice nucleation, in order to account for the temperature, the cooling rate, the saturation, and the water droplet size, two methods have been used: 1) Meyers et al.'s (1992) parameterization and 2) Bigg's parameterization (Pruppacher and Klett 1997). The former predicts the total IN concentration (N_{IN}) per liter of air as a function of the ice supersaturation and the temperature as follows:

$$N_{\text{IN}} = e^{\{a+b[100(\delta_i-1)]\}} + e^{[c+d(273.15-T)]}, \qquad (14)$$

where the first term of the right-hand side of (14) represents the concentration of ice deposition nuclei and the second term represents the concentration of ice contact nuclei. To take into account the droplet size dependence, Bigg's parameterization is used. Using data collected in a laboratory, Bigg determined the median freezing temperature of population of water droplets as a function of mean particle size. The analysis leads to the following expression for the median freezing temperature:

$$T_m = \frac{1}{a}\left\{\ln\left[\left(\frac{a\,\ln 2}{BV}\right) + \ln\left(\frac{\partial T}{\partial t}\right)\right]\right\}, \qquad (15)$$

where a and B are constants and V is the droplet volume. Here a has a mean value of 0.65 $(°C)^{-1}$ and $B = 2.0 \times 10^{-6}$ cm^{-3} s^{-1} for atmospheric water droplets (Pruppacher and Klett 1997). In the model, the median freezing temperature is calculated for each size bin. When $T < T_m$ for a particular size bin, the number of ice crystals nucleated is determined by the parameterization of Meyers et al. (1992). This method for determining IN accounts for the size of water droplets, the temperature, the cooling rate, and the ice supersaturation.

The homogeneous freezing temperature is determined as follows. We assume that pure water droplets freeze at −40°C. Since the homogeneous freezing rate is very high, we assume that droplets freeze instantaneously. If solute is present, the homogeneous freezing temperature can be either prescribed or parameterized as a function of the solute nature and concentration within the droplet. In the model, haze droplets also freeze instantaneously once the homogeneous freezing temperature is reached.

3. Model validation

a. Aerosol microphysics

The microphysics part of the model is validated against observations and other models. For the aerosol part, we compared the model results to the observations of Shaw (1983). Similar aerosol spectrum observations

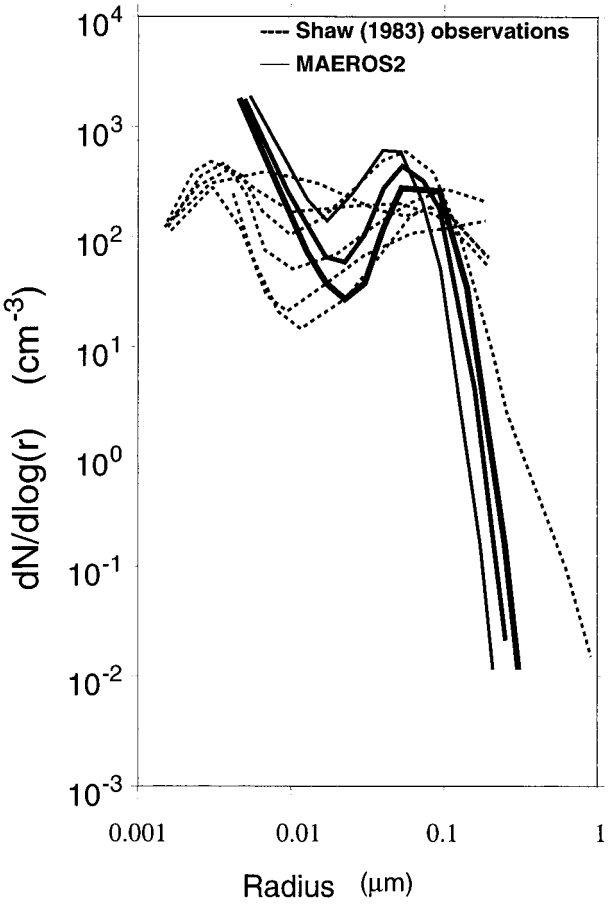

FIG. 1. Observation of Shaw (1983) showing the aerosol size distribution in Alaska during Arctic haze events (dashed lines) and simulation of the aerosol spectrum with MAEROS2 after 10, 15, and 20 days using a constant observed (Shaw 1983) nucleation rate of small aerosols (0.01-μm diameter) of 10^{-18} g cm^{-2} s^{-1}. Initially, there is no aerosol. Spectra obtained with MAEROS2 are the result only of the aerosol coagulation of freshly nucleated aerosols.

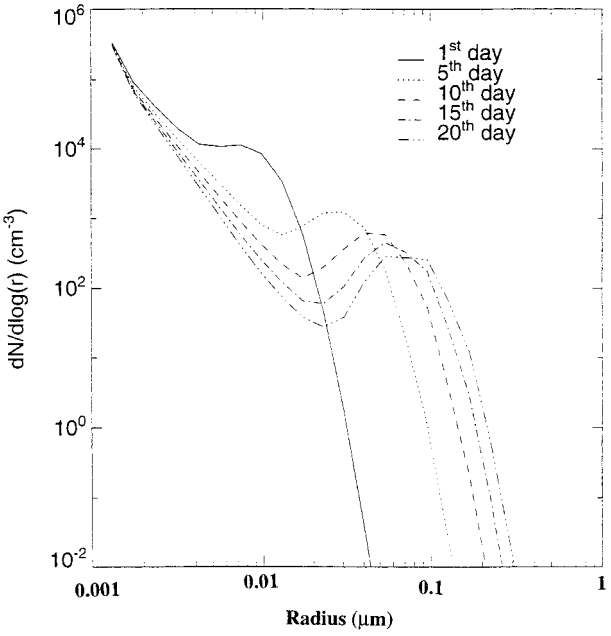

FIG. 2. Aerosol spectrum obtained with MAEROS2 after 1, 5, 10, 15, and 20 days of simulation. In this simulation, a constant flux of aerosol nucleation is assumed at the small end of the spectrum. The accumulation mode is formed only by the coagulation of small particles of the nucleation mode. Twenty days are required to form the accumulation mode.

have also been made by Heintzenberg (1980) and Shaw (1984, 1986). Shaw (1983) has observed aerosol spectra in Alaska during spring in both haze and nonhaze conditions (see Fig. 1). Haze periods are characterized by large concentrations of anthropogenic sulfates from long-range transport.

Observations show two modes: the nucleation mode centered on 0.005 μm and the accumulation mode centered near 0.1 μm. The first mode results from nucleation of new particles by gas-to-particle conversion of sulfuric acid vapor. The accumulation mode is formed by coagulation of Aitken particles from the nucleation mode. This coagulation activity is mostly driven by Brownian motion of the very fine particles. Observations during early spring show a larger concentration of particles in the nucleation mode during Arctic haze events. This is an outstanding characteristic of aged aerosols in midspring at high latitudes where oxidation by photochemistry is initiated (Seinfeld and Pandis 1998). During winter and early spring at high latitudes, without radiation, the oxidation is much slower and particles are partly generated at lower latitudes. Under these conditions the nucleation mode is much smaller.

Shaw (1983) has shown that it takes up to three weeks to form an aged aerosol with the characteristics found in Arctic haze. A 20-day simulation has been performed with the conditions described below to test the timescale required to form each mode as compared to Shaw's observations. The model has been configured as a box model, which is a single volume in which only the aerosol coagulation is simulated. For the purpose of this test, cloud formation as well as radiation have been omitted. Initially, there is no aerosol in the volume. Particles are injected in the volume as a prescribed mass flux at the low end of the spectrum and evolve to larger particles by coagulation only. Figure 2 shows the resulting spectrum after 1, 5, 10, 15, and 20 days. At day 1, the nucleation peak around 0.002 μm is well developed whereas the accumulation mode is still in development stage. Twenty days of integration are necessary to produce a fully developed accumulation mode typical of aged aerosols. The timescales for formation of both nucleation and accumulation peaks are in general agreement with timescales deduced from Shaw's observations. The position of the accumulation mode near 0.1 μm and the peak concentration of about 300 cm^{-3} agree well with observed values of 0.08 μm and between 100 and 500 cm^{-3}, respectively. Also, the minimum between

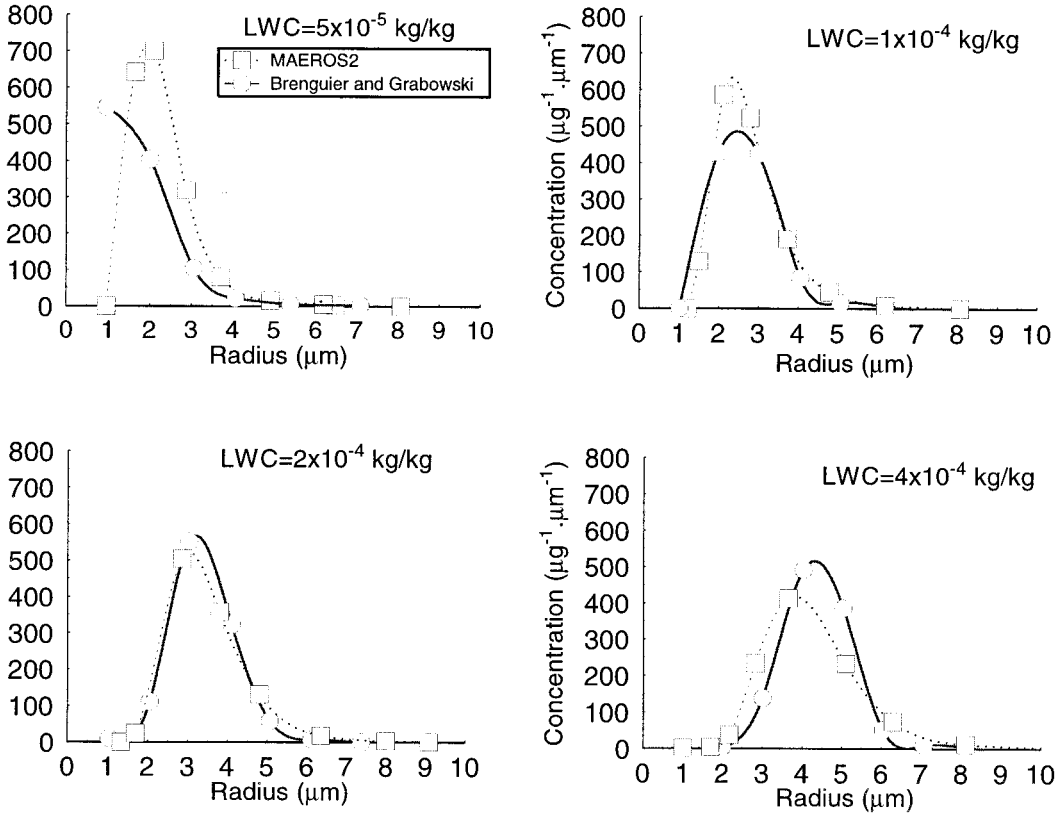

FIG. 3. Cloud spectrum obtained from MAEROS2 and Brenguier (1991) model for four valves of liquid water content.

the two peaks is well reproduced by the model with a concentration value of about 70 cm^{-3} at 0.02-μm radius, compared to observed values varying between 10 and 100 cm^{-3} at 0.01-μm radius. The nucleation peak simulated by the model is somewhat large compared to observations. This is because a constant nucleation rate has been imposed during the integration, which keeps the concentration of newly formed aerosols quite large. In reality, this production of new nuclei is done in great part during the aerosol transport from midlatitudes by photochemistry. Entering the dark winter above the Arctic circle, the aerosol number concentration remains constant or decreases slowly by coagulation and dry and wet deposition, while the concentration of small nuclei decreases rapidly. The slopes of the aerosol size distributions are similar except for radii larger than 0.5 μm. The observed slope is smaller due to the contribution of giant aerosols such as sea salt and dust, which were not considered in our simulation. These comparisons show that the aerosol microphysics of the model produces an aerosol size distribution similar to that observed in aged arctic aerosols.

b. Aerosol–cloud interactions

During the polar night, the lower atmosphere cools radiatively, in the absence of solar radiation. The aerosols serve as nuclei upon which water vapor can condense. The formation of condensate involves the aerosol activation and the cloud particle's microphysical processes such as nucleation, aggregation, coalescence, sedimentation, and water vapor deposition and condensation. To assess our model for these physical processes, we compare the model results with an alternate cloud model and observations.

A comparison with Brenguier's (1991) model has been conducted, which has 30 size bins of equal width for radii between 1 and 12 μm. The high resolution of this model allows for evaluation of the mass diffusion through size bins likely to occur with our model due to the decreasing resolution with size. We use Brenguier's model to compare the cloud spectrum just after aerosol activation. The test consisted of assuming an initial supersaturation over a CN concentration of 1.087×10^6 L^{-1} of radius from 0.1 to 1 μm. Figure 3 shows the comparison of both models after equilibrium state is reached for different supersaturations. Despite discrepancies in the spectrum shape, equivalent radii of both models are similar with differences of less than 6% (see Table 2). Therefore, the lower resolution of the small end of the cloud particle spectrum does not seem to alter significantly the model accuracy in predicting the cloud equivalent radius just after the aerosol activation.

TABLE 2. Equivalent radius of the cloud particle size distribution obtained with MAEROS2 and Brenguier's (1991) model for different amount of condensate.

Condensate mass (g kg^{-1})	r_e Brenguier (μm)	r_e MAEROS2 (μm)	Difference (%)
0.05	3.02	3.10	2.6
0.1	3.34	3.50	4.6
0.2	3.88	4.12	5.8
0.4	4.73	5.01	5.6

The model has also been assessed with observations. Table 3 shows four cases of arctic clouds observed during December 1967 at Barrow, Alaska (Witte 1968). The mean diameter and the standard deviation of the ice crystal spectrum of two stratus cases (flights D and J) and two diamond dust cases (flights A and H) are shown. Witte's (1968) observations indicate that the standard deviation varies from 1.45 to 1.82 with mean diameters from 17 to 42 μm in the cases of stratus and from 31 to 61 μm in the case of diamond dust. The stratus cases show a narrower ice crystal spectrum and smaller mean diameter than the diamond dust cases. Note that in the case of lower latitude marine stratus, Considine and Curry (1996) have obtained similar standard deviations with values ranging from 1.3 to 1.5.

Figure 4 shows the standard deviation of the ice crystal size distribution as a function of the mean diameter at every 450 s for two runs of 8 days performed with MAEROS2 (see section 3a). We have assumed initially an aerosol mass concentration of 5 μg m^{-3}, typical of the arctic conditions during winter and a cooling rate of -2 K day^{-1} for this simulation. All microphysical processes related to aerosols and cloud particles were allowed for. Values of standard deviation obtained with the model are also scattered varying between 1.3 and 1.6 with some values as high as 2.0. These values are similar to the observations of Witte. As will be shown in the next section, the highest values have been obtained as a result of: bimodal ice crystal spectrum formation after a second aerosol activation, sedimentation of large ice crystals from the layers above, and mixed phase cloud in which water droplets are confined to smaller sizes.

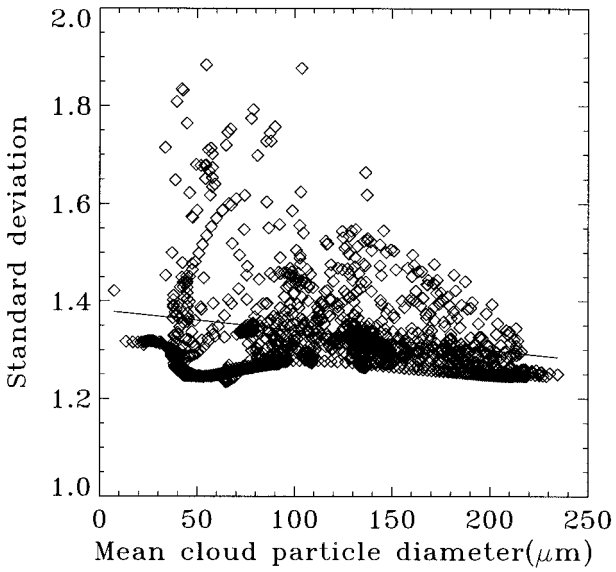

FIG. 4. Standard deviations of the cloud particle size distribution obtained during an 8-day simulation of Arctic diamond dust with MAEROS2. Values of standard deviation are plotted each 450 s.

Comparisons of the model results with both Witte's (1968) observations and Brenguier's (1991) model have shown that the decreasing resolution with increasing size bin does not artificially exaggerate the ice spectrum width by diffusing the mass forward to larger diameters. On the contrary, the model slightly underestimates the cloud spectrum width when compared to Witte's (1968) observations.

4. Application to arctic ice fog and diamond dust

The model has been used to simulate diamond dust precipitation occurring during winter over the Arctic. In this simulation, dynamical forcing and solar radiation are not considered. The goal in this experiment is to focus on microphysical processes acting to form ice crystals under a very cold and stable air mass, such as those observed in the Arctic during winter. Therefore, although idealized, this case is very close to the real atmospheric conditions prevailing over the Arctic Ocean during the cold season. The model allows for the in-

TABLE 3. Atmospheric conditions and cloud microphysical properties calculated based on data compiled by Witte (1968) during three flights over Barrow (Alaska) in Dec 1967.

	Altitude (km)	Temperature (°C)	Presence of liquid phase	Mean diameter (μm)	Standard deviation
Flight H	3.44	-19	No	30.50	1.82
Flight H	2.84	-17	Yes	53.00	1.55
Flight H	2.55	-15	Yes	43.20	1.66
Flight H	1.39	-15	Yes	39.96	1.76
Flight H	0.28	-18	No	60.40	1.55
Flight A	0.15–2.90	-34–-25	No	36.20	1.60
Flight J	3.02	-23	No	16.90	1.45
Flight D	2.0	-23	Yes	41.62	1.75

TABLE 4. Percentage of the ice mixing ratio initially confined at 940 hPa that remains at 940 hPa or sedimentates into the two layers below after 900 s for four different ice crystal mean diameters. Theoretical values and model values are shown. Percentage of ice mixing ratio at the three levels are shown as: 940–970–1000 hPa.

	Theory	Model (three layers)
D = 10 μm	6%–94%–0%	6%–94%–0%
D = 75 μm	48%–52%–0%	55%–38%–7%
D = 100 μm	43%–57%–0%	49%–42%–9%
D = 150 μm	0%–95%–5%	20%–58%–22%

frared radiative cooling of the atmosphere and the subsequent ice crystal and water droplet formation. It simulates the time evolution of both the aerosol and cloud size spectra.

a. Model initialization and assumptions

A simulation of 8 days has been performed with nine vertical levels. Since the microphysics part of the model is very time consuming, the detailed microphysics described in the previous section has been used only in the first three levels above the surface, that is between 940 and 1000 hPa. In the remaining six levels, covering pressure levels between 500 and 940 hPa, a bulk cloud parameterization in which condensed matter precipitates instantaneously onto the ground is used. This method allows for longer simulations and proper treatment of the water vapor mixing ratio in the upper atmosphere. However, the coarse grid resolution may diffuse the mass during the sedimentation process. To evaluate this error, we made the following simple analysis. Let us assume initially that ice crystals are homogeneously distributed in the upper box at 940 hpa and have the same diameter. We calculated the percentage of the ice water content that stays in the first box, goes in the second box (970 hPa), and in the third box (1000 hPa) after 900 s. Table 4 shows the results for three ice crystal sizes assuming an infinite number of levels (theory) and assuming the three levels used in the model. Results indicate that the effect of the coarse resolution is to diffuse numerically the mass both forward and backward. The error remains under 10% for ice crystal diameters smaller than 100 μm. The error increases for larger diameters and reaches 25% at 150-μm diameter. This analysis shows that in diamond dust events, the model is more likely to produce numerical diffusion. In ice fog simulation, small diameters of ice particles gives negligible errors. Since the concentration of ice crystals larger than 100 μm is small (of the order of 1 L^{-1}) (Curry et al. 1990), the error associated to the coarse grid resolution is not expected to significantly alter the results. This is confirmed by the experiment of Girard and Blanchet (2001) who have compared the detailed model used in this study with a parametric model using 48 levels in the vertical. They found a 15% difference in the surface temperature after 12 h between the two models. Considering the fact that the parametric model has a parameterized microphysics that is likely to cause errors in the microphysical fields, it means that the low resolution of the detailed model is responsible for less than 15% error. Therefore, the error caused by the coarse grid remains acceptable in this context.

Initially, the atmosphere has the properties of a subarctic winter maritime air mass as defined by McClatchey et al. (1972). The surface temperature is initially set to -19.8°C. An homogeneous thick sea ice surface is assumed with no open water. Surface temperature time evolution is determined from the surface energy budget by assuming no sensible and latent energy release and a surface emissivity of unity in the infrared. In the Arctic during winter, the sensible heat flux from the atmosphere toward the surface is effective at the beginning of the air mass cooling when the surface is cooler than the air above. However it rapidly decreases to a small value as the air temperature just above the surface cools radiatively and reaches the surface temperature, which is carried out in about one day (Curry 1983). The thick sea ice combined with the absence of solar radiation inhibit the sublimation of the sea ice. The surface acts rather as a water sink. In this context, the simple treatment of the surface is justified. Furthermore, that allows us to focus on microphysical and radiative processes leading to the formation of diamond dust and ice fog, which is the goal of this study. The experiment of Girard and Blanchet (2001) (see above) has also shown small errors when the detailed model is compared to a climate model with a complex surface scheme. Similar to the Curry (1983) method, we simulate the infrared radiative cooling of a mild and moist air mass and its transition toward an arctic air mass in the absence of solar radiation. Regarding the aerosols, we assume an initial lognormal distribution with a mean diameter of 0.2 μm and a standard deviation of 1.3. These values are based on observations taken in the Arctic over the past years (Blanchet and List 1983; Schnell 1984; Shaw 1995). The aerosol nucleation and the chemical processes are not simulated in the model. We assume a constant nucleation rate of 10^{-18} g cm^{-2} s^{-1} at the small end of the aerosol spectrum. This value is based on observations of Shaw (1983). Initially, the aerosol mass concentration is set to 5 μg m^{-3}, which is representative of the Arctic during winter (Barrie 1986).

In the following two sections, two 8-day simulations are analyzed. In the first simulation, pure sulfuric acid aerosol is considered. Aerosols are assumed to be 100% soluble and the homogeneous freezing temperature of haze droplets is a function of acid dilution. An empirical formula based on Bertram et al.'s (1996) laboratory experiment is used. In the second simulation, an internal mixing of a different kind of aerosol is assumed. We have prescribed the solubility to 50% and the homogeneous freezing temperature to 238 K.

b. Diamond dust

Figure 5 shows the aerosol and cloud spectra time evolution in the first layer above the surface. During most of the first day, there is no cloud. However, the aerosol spectrum experiences some changes by coagulation of freshly nucleated particles joining the accumulation mode, leading to a slight concentration increase of the accumulation mode. Because of the longer formation timescale (Shaw 1983), aerosols larger than 0.1 μm remain at about the same concentration. Figure 6 shows that during this period of time, the supersaturation increases as the air cools radiatively. At the end of the first day, the first level above the surface is saturated and cloud particles are nucleated. The aerosol activation leading to the cloud formation can be seen in Fig. 5a where the larger aerosols acting as CN or IN are suddenly removed from the aerosol spectrum. Cloud particle concentration is low with a number concentration on the order of 1000 L^{-1} (see Fig. 7) and an ice water content of about 0.05 g m^{-3} (see Fig. 8) with a mean diameter of about 50 μm (see Fig. 9). These values are similar to observations of diamond dust events in the Arctic (Schnell 1984; Curry et al. 1996, 1999). Figure 10 shows that in this case, all cloud particles are in the liquid phase. Temperature of -13°C and water droplet sizes are not favorable to the formation of ice crystals. Cloud and atmospheric conditions hypothesized to be necessary for the formation of mixed phase clouds will be discussed below.

After the first aerosol activation at 1000 hPa, the cloud spectrum shifts toward larger diameter by the growth in size of water droplets by coalescence and water vapor condensation. Water droplet concentration decreases through gravitational deposition of the largest cloud particles (see Fig. 5). After the initial activation, water droplet number concentration decreases rapidly to 30 L^{-1} and the mass concentration of water droplets is lowered by a factor five. Then, after decreasing suddenly during the aerosol activation, the supersaturation over ice increases one more time. The production of supersaturation depends on the air mass cooling rate and on the deposition rate of water vapor onto activated aerosol particles and cloud particles [see Eq. (6)]. As the cloud droplet number decreases by coalescence and sedimentation, the total condensation rate is reduced. When the concentration of cloud particle is too low to balance the production term, then the supersaturation increases again. Note that this cycle is very rapid for the first activation compared to later aerosol activation events, due to the high cooling rate near the surface at the beginning of the simulation. This rapid cycle and large variability of microphysical variables has been observed in fog type cloud (Pruppacher and Klett 1997) and arctic boundary layer clouds (Curry et al. 1990).

During the first 3 days, other aerosol activations occur only in the lowest model layer around 1000 hPa. The cooling rate remains relatively high at about -5°C day^{-1}, allowing the supersaturation to stay relatively high. However, after the first activation event, the following activation produces fewer cloud particles. Large aerosol present in the initial activation are found in much lower concentration in the following cases. Between each activation event, large aerosols depleted by previous activation are gradually regenerated through aerosol coagulation in the accumulation mode. However, the timescale for the formation of these aerosol is relatively long. Therefore, when activation events occur at high rates, the concentration of large aerosol depleted is low and fewer cloud particles are activated. As a result, the mean diameter of cloud particles is larger. This behavior can be seen in Fig. 5 just after the first activation at 1000 hPa.

At the third day, clouds appear in the second model layer at 970 hPa. The aerosol activations are however much less important in terms of aerosol mass activated than in the case of 1000 hPa because of the lower cooling rate at this level. The supersaturation reaches lower values and the number concentration of activated aerosols is also lower. Meanwhile, at 1000 hPa, ice supersaturation collapses from about 30% to values between 10% and 20% due to condensation on ice crystals falling from the upper layer. Also, the cooling rate at 1000 hPa, which was of about -5°C day^{-1} before, has significantly decreased as the emissivity of the layer above has increased due to the cloud formation at this level.

The infrared cooling of the atmospheric column resumes and condensate appears in the third layer above the ground (940 hPa) at day 5. The infrared cooling rate is relatively small as compared to the lower layers at their development phase. As a result, supersaturation increases more slowly and aerosol activation events are less frequent (see Fig. 6). From days 5 to 8, the source of ice crystals at 970 hPa and at 1000 hPa is mainly the sedimentation of ice crystals nucleated aloft. This situation allows the regeneration of the aerosol spectrum in the lower levels and gives rise to a characteristic vertical structure of the boundary layer cloud. Most of the cloud particles are nucleated at the cloud top while below, existing ice crystals mostly come from precipitation of ice crystals nucleated in upper layers. Falling ice crystals grow by water vapor deposition and to a lesser extent by aggregation. As a result, ice crystals at the top of the cloud are smaller and more numerous while the ice crystal number concentration is much smaller in the lower layers and particles are larger. An example of this vertical structure has been reported by Pinto (1998) during the Beaufort and Arctic Storm Experiment (BASE) in October 1994.

1) SUPERSATURATION RELAXATION TIME

Figure 6 shows that ice supersaturation is permanently positive, reaching values as high as 40%. High supersaturation is a characteristic of diamond dust events. Curry et al. (1990) reports supersaturation over

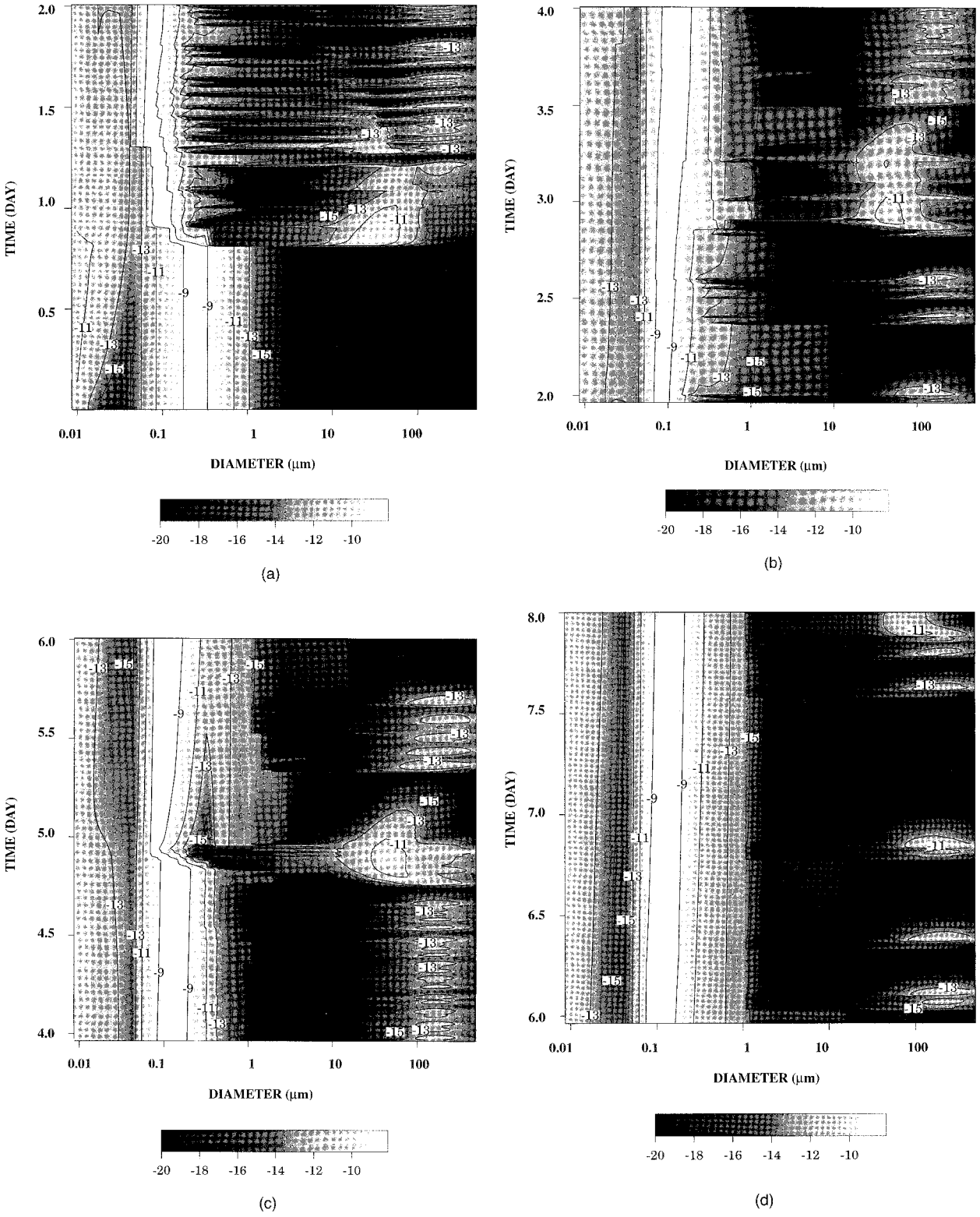

FIG. 5. Logarithm of the aerosol mass size distribution at 1000 hPa for the diamond dust simulation for (a) days 0–2, (b) 2–4, (c) 4–6, and (d) 6–8. Large values for diameter larger than 1 μm indicate the aerosol mass contained within cloud droplets and ice crystals.

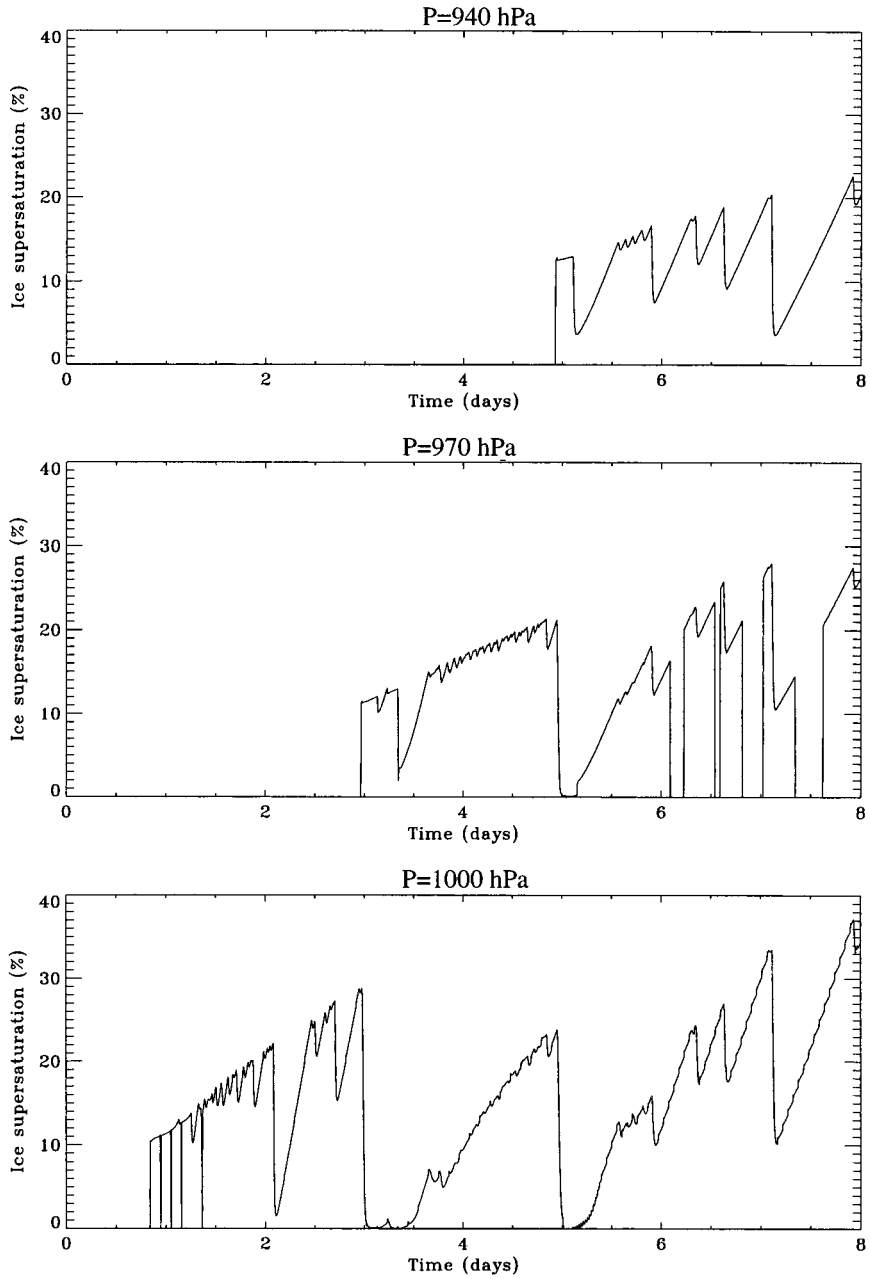

FIG. 6. Time series of ice supersaturation at the three first levels above the ground.

ice varying between 10% and 30% in more than 80% of the diamond dust cases observed during the Arctic Gas and Aerosol Sampling Program (AGASP). In April 1992, ice supersaturation just above the sea ice surface was common during the Lead Experiment (LEADEX) (Ruffieux et al. 1995). In December 1967, Witte (1968) also observed high ice supersaturation in Point Barrow, Alaska. This feature is also present in other cloud types such as cirrus in midlatitudes (Khvorostyanov and Sassen 1998b) and arctic stratus (Curry et al. 1990; Curry and Radke 1993; Pinto 1998).

Allowing for ice supersaturation in climate models is important for a proper cloud parameterization. Neglecting supersaturation can result in substantial overestimation of the cloud ice and water content and consequently, considerably affect the cloud–radiative effect.

Khvorostyanov and Sassen (1998a) have suggested using a supersaturation relaxation time τ for determining the persistence of ice supersaturation in clouds. It is defined as the time required for the ice supersaturation $\Delta = \delta - 1$ to decrease by a factor e; that is,

$$\Delta(t) = \Delta(t_0) \exp(-t/\tau). \quad (16)$$

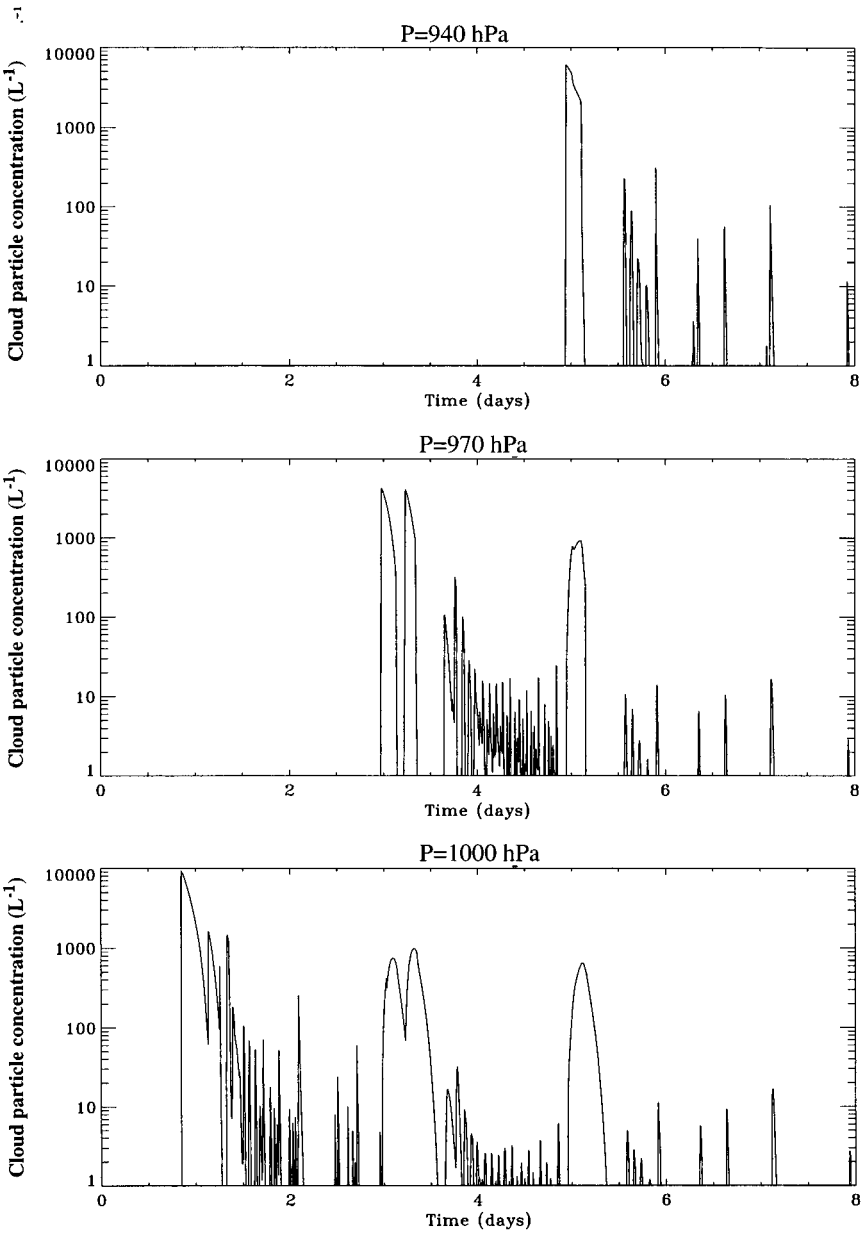

FIG. 7. Time series of cloud particle number concentration (L^{-1}) at the three first levels above the ground.

Assuming a mixed-phase cloud, the ice supersaturation relaxation time can be expressed as a function of the number concentration of ice crystals and water droplets and their mean diameters as follows:

$$\tau = \left[4\pi D(\overline{N_W}\,\overline{r_W} + \overline{N_I}\,\overline{C_I})\right]^{-1}. \quad (17)$$

Figure 11 shows the supersaturation relaxation time for the simulated diamond dust case. Very high values in the 1–100 h range are obtained. These values are much higher than those obtained for cirrus clouds (e.g., Khvorostyanov and Sassen 1998b). The very low ice crystal concentration characterizing diamond dust events is the main contributing factor [second term of the right-hand side of (17)]. Ice concentration of a few crystals per liter is obtained most of the time (see Fig. 7). The few times number concentration increases to the order of 100 L^{-1} corresponds to a substantial reduction in the supersaturation relaxation time from over 10 h to less than 5 h.

2) MIXED-PHASE IN DIAMOND DUST EVENTS

Mixed-phase clouds are very common in the Arctic and are the most difficult to simulate in climate models.

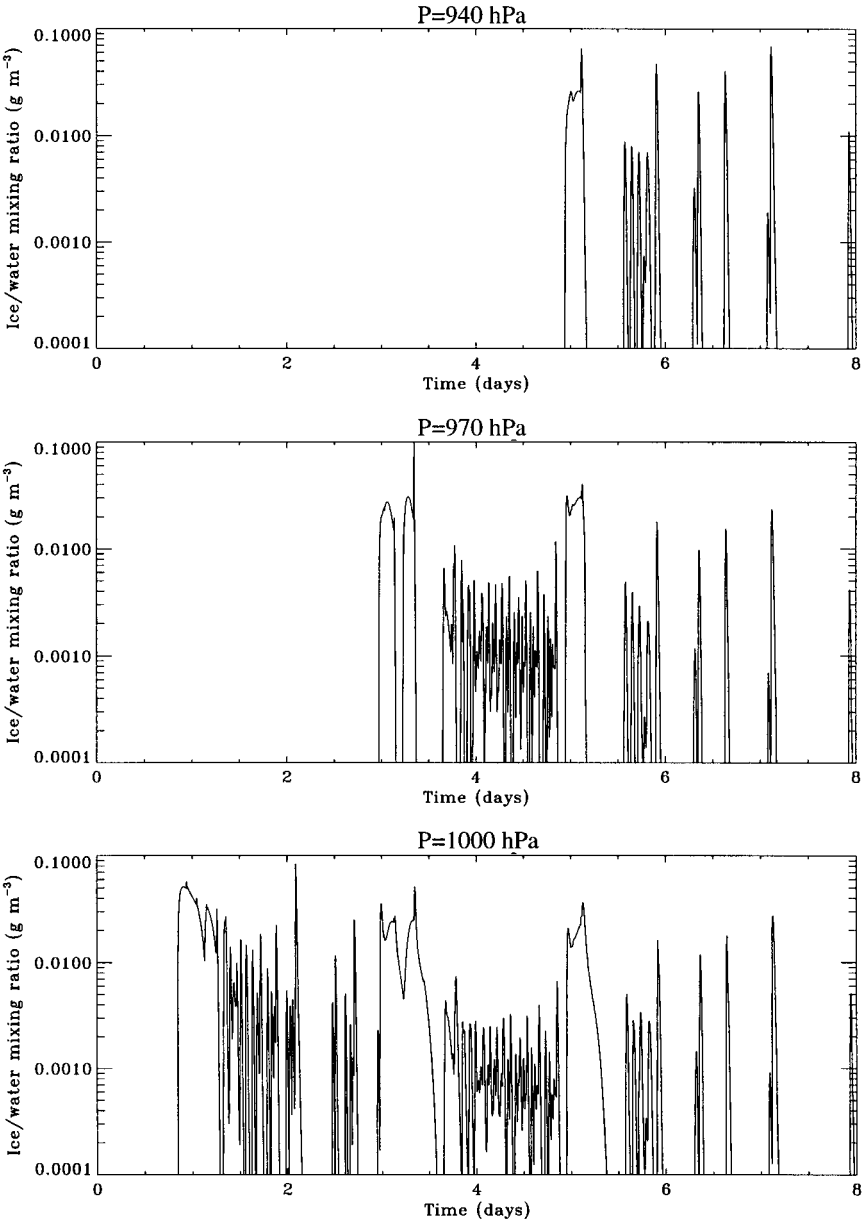

FIG. 8. Time series of cloud mixing ratio (g m^{-3}) at the three first levels above the ground.

The importance of properly simulating these clouds in climate models has been addressed by Gregory and Morris (1996).

To address the formation and maintenance of mixed-phase clouds in stable boundary layer clouds such as diamond dust, MAEROS2 and observations are used. Figure 10 shows the ice crystal proportion to the total cloud particles as a function of time for three levels above the ground. At 1000 hPa, only water droplets are nucleated during the initial aerosol activations. The temperature is then relatively warm at -10°C and water droplet diameters are of the order of 10 μm. At hour 30, ice crystals appear and increase in proportion up to 100% at hour 50. In the first level, there is no other water droplet nucleated after hour 50. In the upper levels, the pattern is similar except that ice crystals appear later and the phase transition period is longer. At 970 hPa, ice crystals are nucleated for the first time at hour 87 and the transition period lasts for almost 2 days. Finally, at 940 hPa, ice crystals initiate at hour 120 and mixed-phase period lasts almost 3 days with some episodes with water droplets or ice crystals only. While the ice proportion increases gradually at 970 hPa, the two other levels experience a much more noisy increase. That is due to the activation cycle in the second level. Indeed, the high frequency of small aerosol activation

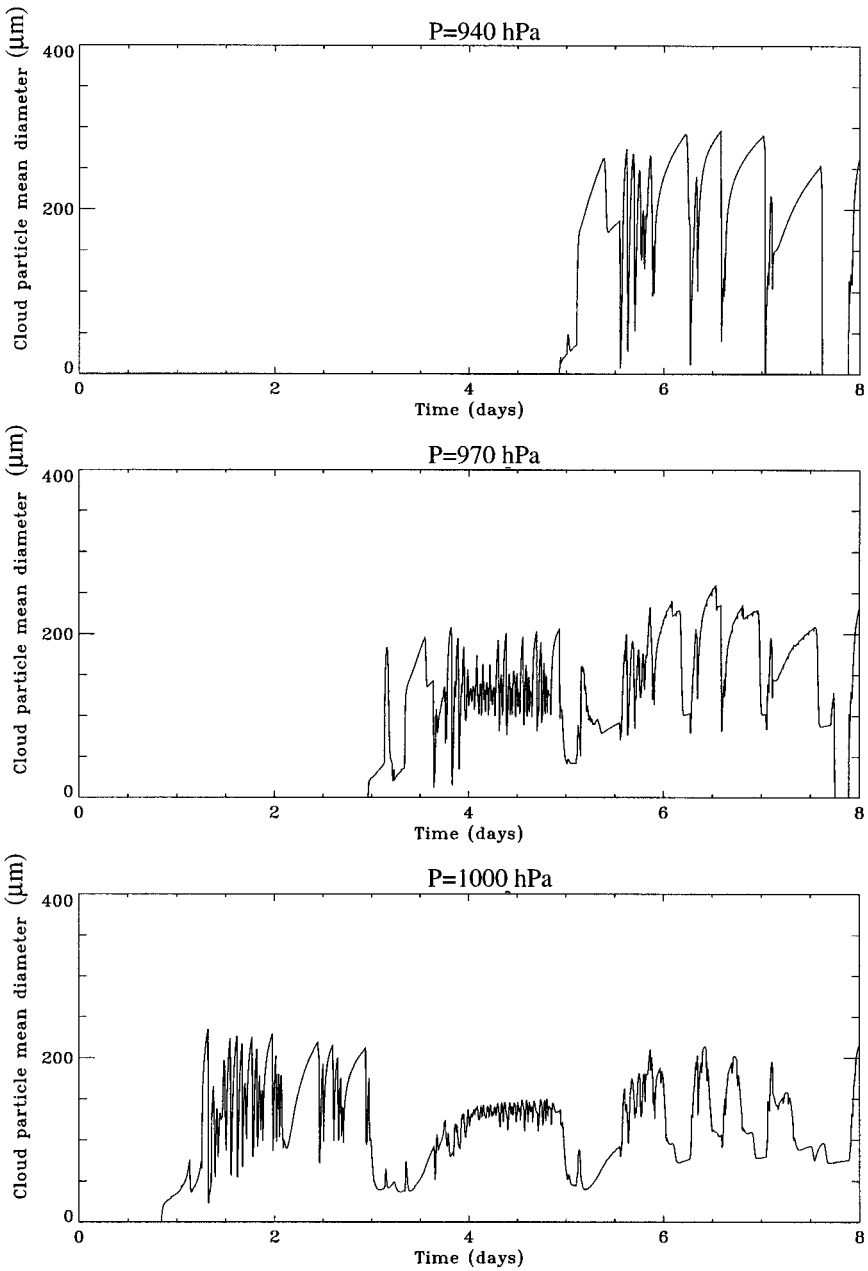

FIG. 9. Time series of cloud particle mean diameter (μm) at the three first levels above the ground.

at 970 hPa produces less variability of the mean cloud particle diameter. Since the heterogeneous freezing depends on cloud particle size, the ice proportion does not experience dramatic change after an activation. At 1000 and 940 hPa, the mean diameter of cloud particles experiences larger variation due to larger aerosol activation events producing smaller cloud particles that freeze at low temperatures. In these cases, the ice proportion can sometimes drop from 100% to very low value.

These results suggest a vertical structure of the mixed phase stable clouds with most of the liquid phase in the upper part of the cloud. This behavior can be explained as follows. The upper part of the cloud experiences large infrared cooling rate due to increasing emissivity. Supersaturation increases rapidly and allows for further CN activation, thus producing many water droplets too small to nucleate to ice. This situation remains as long as the temperature is above the heterogeneous ice nucleation temperature of small water droplets as given by (15). The natural instability produced by the presence of both phases leading to the so-called Bergeron effect is quite ineffective in this case because of the very low

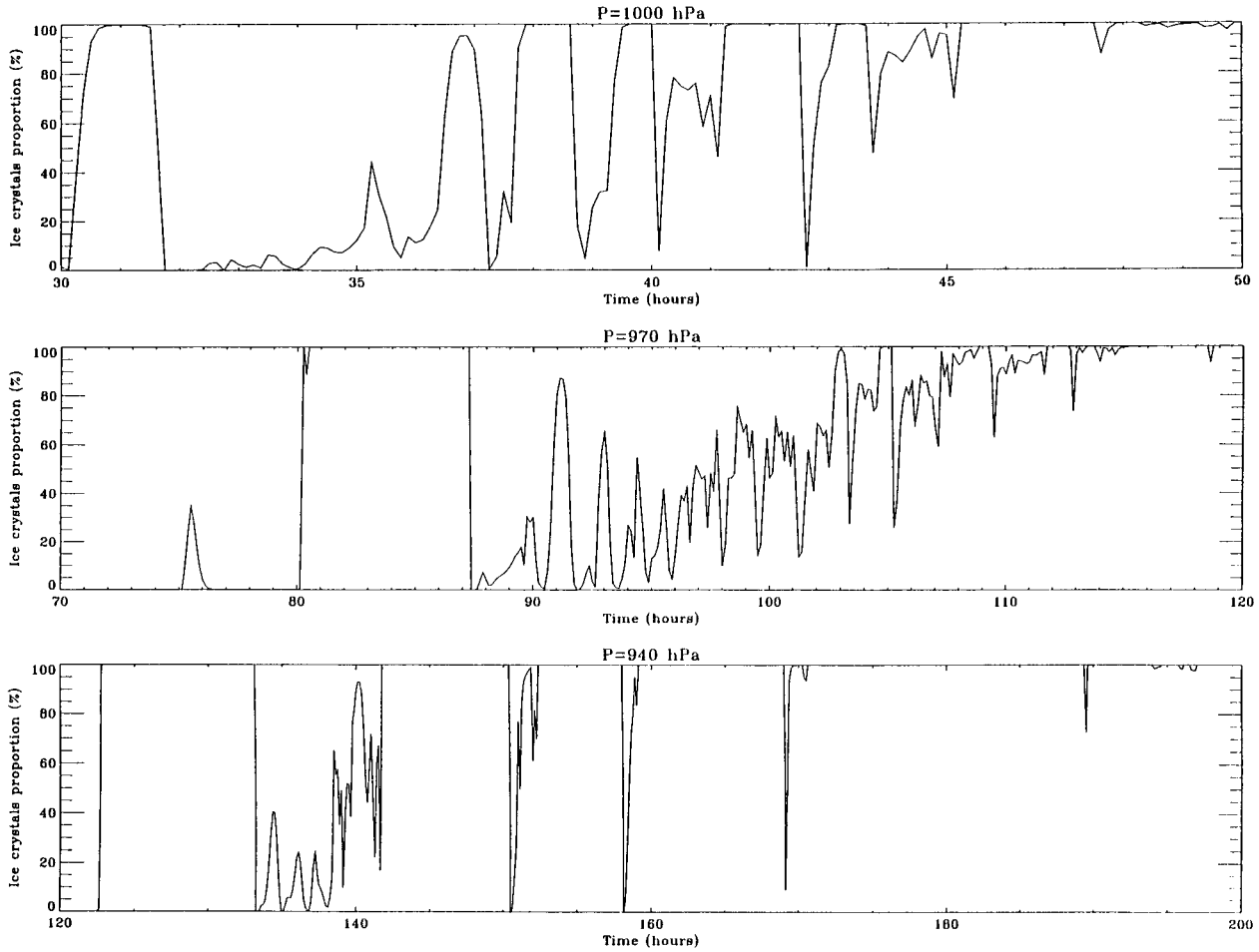

FIG. 10. Time series of the cloud phase indicated here by the ice crystal mass proportion at the three first levels above the ground.

ice crystal number concentration. Indeed, total rate of water vapor absorption by ice crystals is lower than evaporation rate of water droplets. In this case, water droplets evaporate until water saturation is reached. Afterward, water droplet evaporation rate is controlled by the ice crystal concentration. This may allow mixed-phase clouds to persist for extended periods of time. In the present case, the transition period increases with height due to the lower concentration of ice crystals in the highest levels.

Observations seem to confirm this behavior. Most of liquid droplet mass was observed in the upper layers of the diamond dust event in October 1994 in Alaska (Pinto 1998). This feature has also been observed in several cases of low thin stratus clouds during the FIRE Arctic Cloud Experiment in May 1998 (Curry et al. 2000). Witte (1968) and Pinto et al. (1997) also report similar vertical structure in arctic mixed-phase clouds. Furthermore, liquid droplets are mostly confined to the smaller end of the cloud spectrum. For instance, Curry et al. (2000) report droplet diameters on the order of 10 μm and ice crystal diameters larger than 100 μm.

Witte (1968) suggested that the absence of water droplets in lower layers could be due to the ice crystal sedimentation from upper levels, commonly called ''cloud seeding.'' Our results show the same behavior. For example, Fig. 6 shows that, at day 3 just after the ice crystal nucleation at 970 hPa event, the newly formed ice crystals fall through the lowest layer and supersaturation decreases from water uptake by ice crystals combined to lower infrared cooling rates. As a result, further aerosol activation is inhibited. In other cases, like in days 5–8, where the ice crystal production rate is weaker at 940 hPa, concentration of ice crystal falling through lower layers is too small to significantly affect the supersturation. However, it seems to be sufficient to stop the supersaturation from rising and consequently to prohibit further major aerosol activations that produce water droplets.

Other factors can be invoked to explain the observed weak concentration of water droplets in low levels. The low temperature required for diamond dust formation is an important factor. In this simulation, temperatures at 1000 and 970 hPa at day 5 are, respectively, -33°C and -23°C. According to laboratory experiments that have lead to (15), water droplets larger than 30 μm in di-

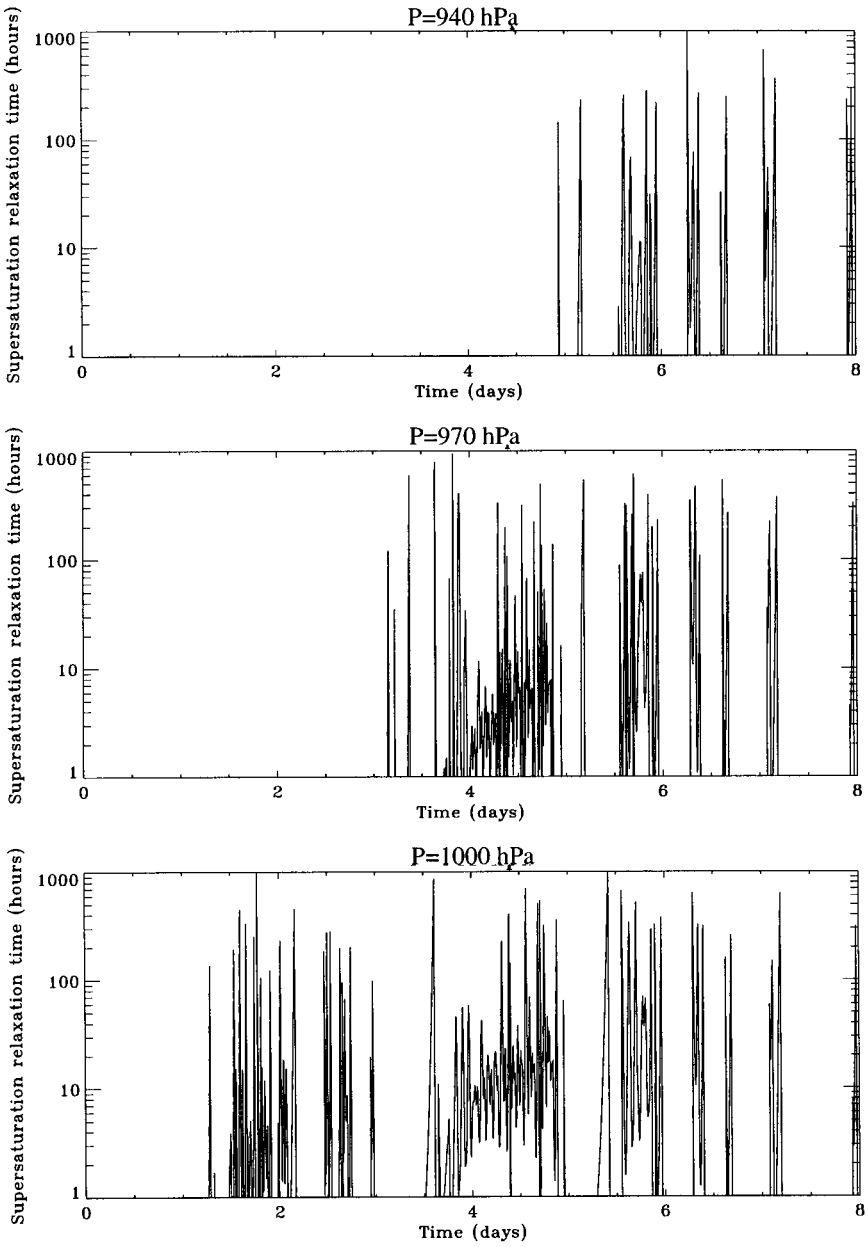

FIG. 11. Time series of the supersaturation relaxation time (hours) at the three first levels above the ground.

ameter can freeze at these temperatures. However, the activation of many aerosol particles is necessary to provide sufficiently small cloud droplets to prevent freezing. Due to the weak cooling rate at the cloud base, this situation does not occur in our simulation.

Witte's (1968) measurements in two diamond dust cases seems to show a temperature dependence. Table 3 shows two cases of observed extended diamond dust events (flight A and H). During flight A, no water phase was observed while during flight H, mixed phase was reported in the middle section of the cloud (between 1.39 and 2.84 km), suggesting a temperature dependence. Indeed, during flight A temperature was below $-25°C$ while during flight H temperatures ranged between $-15°C$ and $-19°C$.

The aerosol composition is a determinant for both heterogeneous and homogeneous ice nucleation. Borys (1989) has observed that IN concentration is decreased by one to four orders of magnitude in Arctic haze event as opposed to pristine conditions. Curry et al. (1996) hypothesized that the sulfuric acid–enriched aerosol, dominant in Arctic haze events, could deactivate IN through collision process. This process can lead to persistence of liquid phase in diamond dust events at very

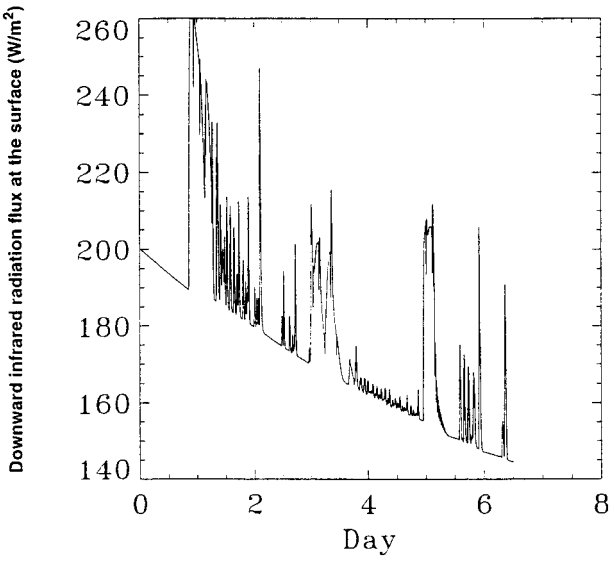

FIG. 12. Downward infrared radiation flux at the surface. Contribution by diamond dusts is illustrated by peaks that increase the infrared flux up to 60 W m^{-2}.

low temperatures that occur in the surface-based temperature inversion commonly observed in the Arctic.

Radiative effects of diamond dust on downward infrared radiation flux at the surface is substantial. Figure 12 shows that diamond dust can contribute as much as 60 W m^{-2} to the downward infrared flux at the surface. Atmospheric cooling with time leads to a main tendency of this radiative flux to decrease. However, nucleation of ice crystals and water droplets forming diamond dust episodically increases the infrared (IR) downward surface flux. This increase depends on the atmospheric liquid or ice water path. Model simulations are in agreement with observed perturbations of IR radiation at the surface during diamond dust events. Witte (1968) observed infrared surface flux increasing up to 80 W m^{-2} in Barrow during winter 1967. Increases of the infrared fluxes ranging from 10 to 40 W m^{-2} have been observed also during the Coordinated Eastern Arctic Experiment during November 1988 (Overland and Guest 1991; Curry et al. 1996).

c. Ice fog

Ice fog is distinguished from diamond dust by the high concentration of ice crystal of smaller diameters. In ice fog, ice crystals are generally closer to spherical shape and their number concentration exceeds 1000 L^{-1} while their mean diameter is below 30 μm. According to Benson (1970) and Bowling (1975), ice fog mostly forms near populated northern areas where strong temperature inversions often near topography causes the air to stagnate. Supply of humidity and IN provided by these cities favor the formation of ice fog. According to Thuman and Robinson (1954), ice fog occurs at temperatures below −30°C, resulting from the homogeneous freezing of haze droplets. This hypothesis may explain the ice fog weekly mean frequency of 11% observed at the remote region of Alert in northern Canada during 1991–94 (Girard and Blanchet 2001). More recently, very high IN concentrations have been observed locally a few meters above the Beaufort Sea and downwind of open leads in the sea ice during Spring 1998 during the SHEBA experiment (Rogers et al. 2000). It has been hypothesized that IN originating from phytoplankton in the sea might be the cause of these high concentrations. This phenomenon might be responsible of the ice fog formation at relatively high temperatures during spring. For instance, spring ice fog has been observed over Alert at frequencies up to 40% under temperatures as high as −10°C (Girard 1998; Girard and Blanchet 2001).

We used MAEROS2 to simulate winter ice fog by the homogeneous freezing of haze droplets. In this simulation, we assume a homogeneous freezing temperature of 238 K. Figure 13 shows ice crystal number and mass concentration, ice supersaturation, and ice crystal mean diameter in the first layer above the ground from day 5 to day 8. From hour 120 to hour 130, temperature at this level has not yet reached 238 K and the situation is identical to the previous simulation where only diamond dust forms, with low ice crystal concentration, large mean diameter, and high ice supersaturation. At hour 130, the temperature falls below 238 K. At this point, the homogeneous freezing temperature of haze droplets is reached and unactivated freezing haze droplets act as IN. The largest aerosol particles are then activated and grow rapidly to ice crystals. At the same time, ice supersaturation, which was high previously, collapses at that point due to the sudden IN availability provided by the haze droplet freezing. The ice crystal number concentration then increases above 1000 L^{-1}. The ice crystal mean diameter decreases dramatically between 10 and 30 μm while the ice crystal mass concentration exceeds 0.01 g m^{-3}. These microphysical properties are typical of ice fogs (Benson 1970; Bowling 1975; Curry et al. 1990).

The main feature distinguishing the time evolution of diamond dust and ice fog is the weak variability of microphysical parameters for ice fog. The large volume of aerosol activations leads to the formation of a large number of small ice crystals in ice fog. The ice crystal aggregation efficiency for 10-μm diameter is low and the sedimentation velocity is very small. As a result, ice fog evolves slowly and may persist many hours. Figure 14 shows that more than 24 h separates the two first major aerosol activations. In the diamond dust simulation, this time was much shorter varying from a few minutes to a few hours. Large ice crystal number concentration results in a low ice supersaturation and a short relaxation time. Figure 15 shows that the relaxation time varies between 0.1 and 1 h in ice fog as opposed to more than 10 h for diamond dust. Supersaturation re-

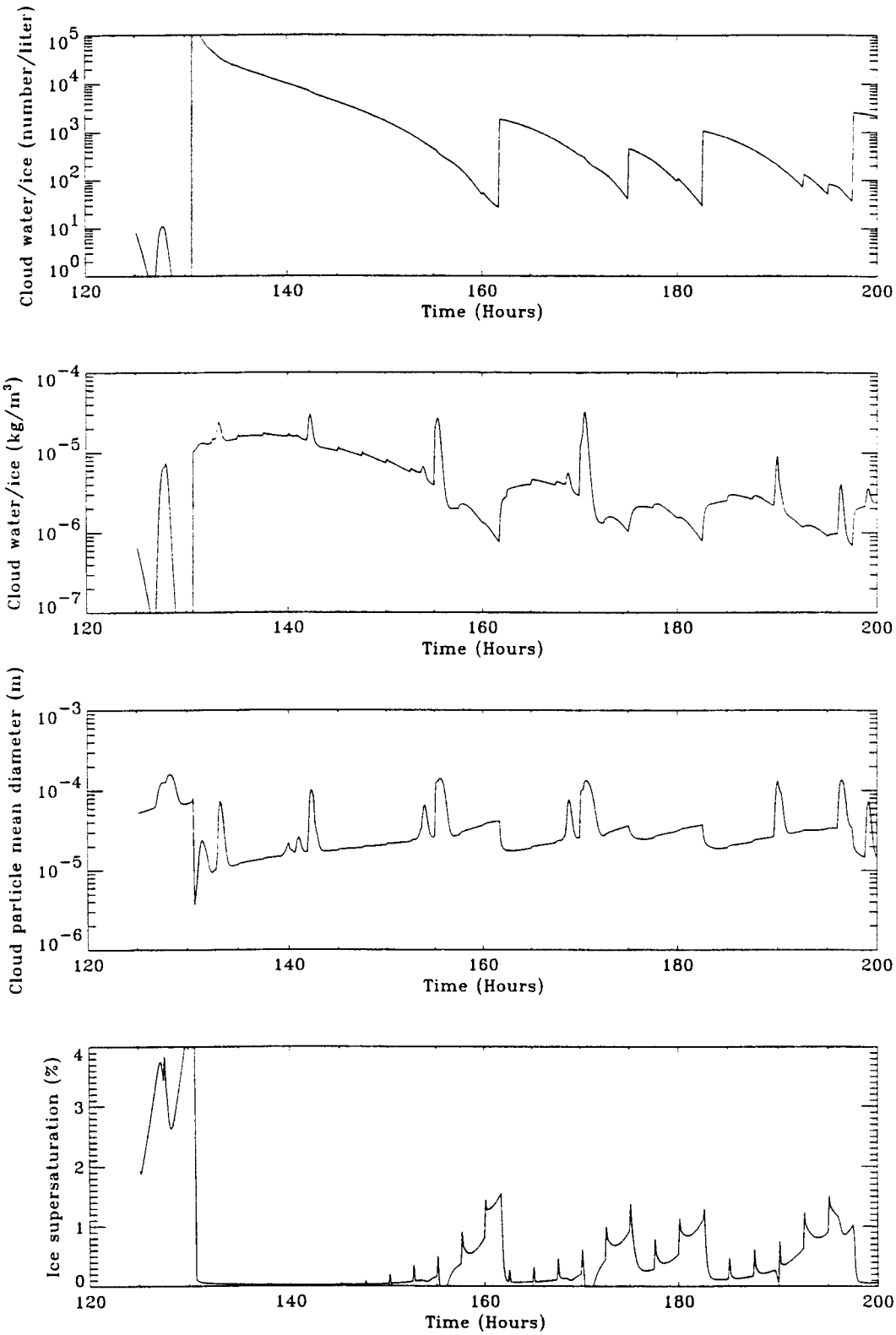

FIG. 13. Time series of ice supersaturation, cloud particle mean diameter (meters), cloud mixing ratio (in Kg m^{-3}), and cloud particle number concentration (L^{-1}) at 1000 hPa for the ice fog simulation.

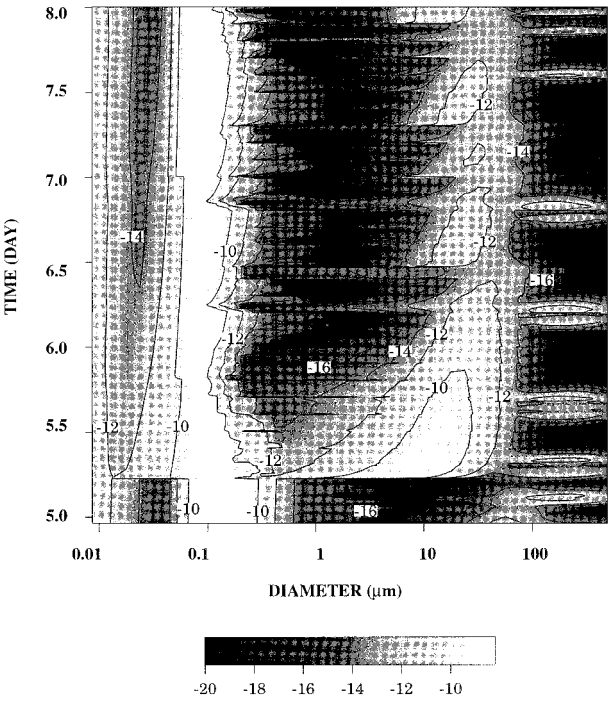

FIG. 14. Logarithm of the aerosol mass size distribution at 1000 hPa for the ice fog simulation. Large values for diameter larger than 1 μm indicate the aerosol mass contained within cloud droplets and ice crystals.

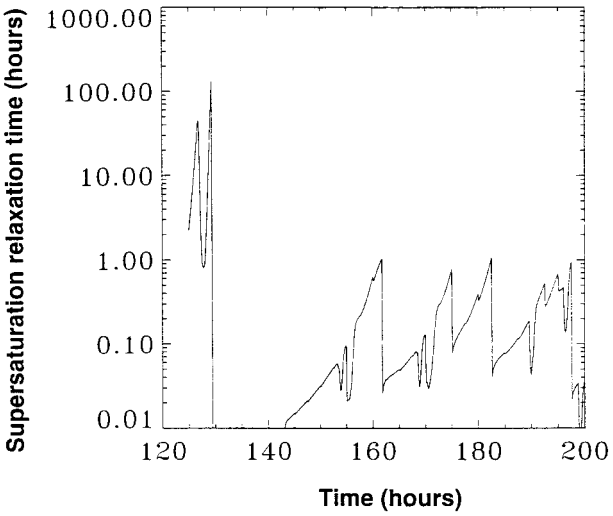

FIG. 15. Supersaturation relaxation time at 1000 hPa for the ice fog simulation. Note the collapse of the relaxation time when ice fog forms at hour 120.

laxation time in ice fogs is similar to that of cirrus clouds (Khvorostyanov and Sassen 1998b).

The radiative effect of ice fogs is larger than for diamond dust due to their extensive lifetime. Table 5 shows the mean downward longwave radiation flux at the surface for the three last days of integration. In the case of ice fog, the mean downward infrared radiation flux at the surface increases by 7.4 W m^{-2}. In terms of temperature, this results in a reduction of the surface cooling rate of about 0.3 K day^{-1}. As a result, the ice fog formation keeps the surface temperature at about 1 K warmer after 3 days of simulation.

5. Conclusions

A comprehensive aerosol–cloud model based on an explicit microphysics model is presented. This modified version of MAEROS2 simulates aerosol–cloud processes, in particular the formation, the evolution, and the dissipation of optically thin clouds like diamond dust, ice fog, or thin stratus or cirrus. The simulated microphysical processes are for aerosols: coagulation, dry deposition, and activation; for cloud water droplets: coalescence, sedimentation, and condensation; and for ice crystals: aggregation, sedimentation, and deposition. Additionally, the model can handle mixed-phase clouds and the Bergeron effect. Turbulence, entrainment, and microphysical processes leading to the formation of graupel, rain droplets, and snow are not accounted for.

The model has been used to simulate the infrared cooling rate of the atmosphere in the Arctic during winter and the associated formation of diamond dust and ice fog. Results highlighted some important factors characterizing these phenomena both on the microphysical and radiative aspect.

The ice supersaturation relaxation time, defined as the time required for the supersaturation to decrease by a factor *e,* generally exceeds 10 h in diamond dust events. In ice fog cases, the relaxation time is less than an hour and similar to values found in cirrus cloud by Khvorostyanov and Sassen (1998b). This notion, first introduced by Khvorostyanov and Sassen (1998a), is useful to parameterize low-level ice clouds in climate models. It provides evaluation for growth rate of ice crystal and a treatment of supersaturation. Relaxation time varies as a function of cloud particle diameter and number concentration. From a climatic point of view, long lasting clouds like cirrus, contrails, stratus, fog, and diamond dust are more important radiatively and must be adequately represented in climate models. The supersaturation relaxation time then becomes a useful concept to parameterize these clouds.

Despite the colloidally unstable nature of mixed-phase clouds, this state can last several days during diamond dust events. The time period during which

TABLE 5. Downward infrared radiation to the surface and surface cooling rate averaged over 3-day simulation with MAEROS2 of a diamond dust and ice fog event.

	Downward IR radiation flux (W m^{-2})	Surface cooling rate (K day^{-1})
Diamond dust	158.33	−2.85
Ice fog	165.79	−2.57

mixed phase is present is controlled by temperature, water droplet volume, and number concentration of ice crystals. In large-scale diamond dust event, the atmosphere cools radiatively. This process is very slow with a cooling rate of the order of 2 K day^{-1}. Observations and our simulation have shown that ice crystals are mainly confined to the largest cloud particles with small number concentration, whereas cloud water droplets are generally small and numerous. In these conditions, the Bergeron process is not very efficient since ice crystals are not sufficient to absorb excess vapor pressure produced by the evaporation of water droplets. As a result, the atmospheric humidity increases up to water saturation. Then ice supersaturation remains very high and mixed-phase condition persists. The model has shown that this unstable equilibrium is broken when finally sufficient ice crystals are formed. That occurs only when the temperature becomes sufficiently low to allow the heterogeneous freezing of the largest water droplets forming diamond dust.

Diamond dust and ice fog have been observed to occur at a frequency of more than 40% in the Arctic during winter. Because solar radiation is a very minor contributor to the surface budget of the Arctic during winter, the surface radiation flux is determined only by the infrared radiation. In such a very cold environment, the clear sky infrared radiation is very low. Consequently, cloud leads to a substantial increase of the downward infrared flux at the surface. Simulations done with MAEROS2 shows that the contribution of diamond dust and ice fog may be as high as 60 W m^{-2}. This result is in agreement with Witte's (1968) observation during winter 1967 in Alaska. Considering the frequency of these clouds during winter in the Arctic, it is essential to include them in a climate model in order to properly simulate the arctic climate and climate change.

Acknowledgments. This work was funded by AES through the NARCM project. The authors would like to thank Judith A. Curry for her useful comments on the manuscript.

REFERENCES

Bailey, M., and J. Hallett, 1998: Laboratory investigation of ice growth from the vapor under cirrus conditions between −30°C and −70°C. Preprints, *14th Conf. on Cloud Physics,* Everett, WA, Amer. Meteor. Soc., 434–437.

Barrie, L. A., 1986: Arctic air pollution: An overview of current knowledge. *Atmos. Environ.,* **20,** 643–663.

Benson, C. S., 1970: Ice fog. *Weather,* **25,** 11–18.

Bertram, A. K., D. D. Patterson, and J. J. Sloan, 1996: Mechanisms and temperature for the freezing of sulphuric acid aerosols measured by FTIR extinction spectroscopy. *J. Phys. Chem.,* **100,** 2376–2383.

Blanchet, J.-P., and R. List, 1983: Estimation of optical properties of Arctic haze using a numerical model. *Atmos.–Ocean,* **21,** 444–465.

——, and E. Girard, 1994: Arctic greenhouse cooling. *Nature,* **371,** 383.

——, and ——, 1995: Water-vapor temperature feedback in the formation of continental Arctic air: Implications for climate. *Sci. Total Environ.,* **160/161,** 793–802.

Borys, R. D., 1989: Studies of ice nucleation by arctic aerosols on AGASP-II. *J. Atmos. Chem.,* **9,** 169–185.

Bowling, S. A., 1975: The effect of ice fog on thermal stability. *North. Eng.,* **7,** 32–40.

Brenguier, J. L., 1991: Parameterization of the condensation process: A theoritical approach. *J. Atmos. Sci.,* **48,** 264–282.

Considine, G., and J. A. Curry, 1996: A stastistical model of drop-size spectra for stratocumulus clouds. *Quart. J. Roy. Meteor. Soc.,* **122,** 611–634.

Curry, J. A., 1983: On the formation of continental polar air. *J. Atmos. Sci.,* **40,** 2278–2292.

——, and L. F. Radke, 1993: Possible role of ice crystals in ozone destruction of the lower Arctic atmosphere. *Atmos. Environ.,* **27A,** 2873–2879.

——, F. G. Meyers, L. F. Radke, C. A. Brock, and E. E. Ebert, 1990: Occurrence and characteristics of lower tropospheric ice crystals in the Arctic. *Int. J. Climatol.,* **10,** 749–764.

——, W. B. Rossow, D. Randall, and J. L. Schramm, 1996: Overview of Arctic cloud and radiation characteristics. *J. Climate,* **9,** 1731–1764.

——, and Coauthors, 2000: FIRE Arctic Cloud Experiment. *Bull. Amer. Meteor. Soc.,* **81,** 5–29.

Fuch, N. A., and A. G. Sutugin, 1971: *High Dispersed Aerosols, Topics in Current Aerosol Research (Part 2).* Pergammon, 200 pp.

Gelbard, F., Y. Tambour, and J. H. Seinfeld, 1980: Sectional representation for simulating aerosol dynamics. *J. Colloid Interface Sci.,* **76,** 541–556.

Girard, E., 1998: Étude d'un effet indirect des aérosols acides en Arctique: Le cycle de déshydratation. Ph.D. thesis, McGill University, 311 pp.

——, and J.-P. Banchet, 2001. Microphysical parameterization of Arctic diamond dust, ice fog, and thin stratus for climate models. *J. Amos. Sci.,* **58,** 1181–1198.

Gregory, D., and D. Morris, 1996: The sensitivity of climate simulations to the specification of mixed-phase clouds. *Climate Dyn.,* **12,** 641–651.

Heintzenberg, J., 1980: Particle size distribution and optical properties of Arctic haze. *Tellus,* **32,** 251–260.

Heymsfield, A., 1972: Ice crystal terminal velocities. *J. Atmos. Sci.,* **29,** 1348–1357.

——, and R. M. Sabin, 1989: Cirrus crystal nucleation by homogeneous freezing of solution droplets. *J. Atmos. Sci.,* **46,** 2252–2264.

Hoff, R. M., 1988: Vertical structure of Arctic haze observed by lidar. *J. Appl. Meteor.,* **27,** 125–139.

——, and W. R. Leaitch, 1989: Ground-based cirrus clouds in the Arctic. Preprints, *Symp. on the Role of Clouds in Atmospheric Chemistry and Global Climate,* Anaheim, CA, Amer. Meteor. Soc., 324–327.

Hu, Z., R. T. Bruintjes, and E. A. Betterton, 1998: Sensitivity of cloud droplet growth to collision and coalescence efficiencies in a parcel method. *J. Atmos. Sci.,* **55,** 2502–2515.

Jayaweera, K. O. L. F., and T. Ohtake, 1973: Concentration of ice crystals in Arctic stratus clouds. *J. Rech. Atmos.,* **7,** 199–207.

Joseph, J. H., W. J. Wiscombe, and J. A. Weinman, 1976: The delta-Eddington approximation for radiative flux transfer. *J. Atmos. Sci.,* **33,** 2452–2459.

Khvorostyanov, V. I., and K. Sassen, 1998a: Cirrus cloud simulation using explicit microphysics and radiation. Part I: Model description. *J. Atmos. Sci.,* **55,** 1808–1821.

——, and ——, 1998b: Cirrus cloud simulation using explicit microphysics and radiation. Part II: Microphysics, vapor and ice mass budgets, and optical and radiative properties. *J. Atmos. Sci.,* **55,** 1822–1845.

Maxwell, J. B., 1982: Climate of the Canadian Arctic islands and adjacent water. *Climatol. Stud.,* **30,** 34–52.

McClatchey, R. A., R. W. Fenn, J. E. A. Selby, F. E. Volz, and J. S.

Garing, 1972: Optical properties of the atmosphere. 3d ed. AFCRL-72-0497, Environmental Research Papers 411, Air Force Systems Command, U.S. Air Force, 108 pp.

McFarlane, N. A., G. J. Boer, J.-P. Blanchet, and M. Lazare, 1992: The Canadian Climate Center second-generation general circulation model and its equilibrium climate. *J. Climate,* **5,** 1013–1044.

Meyers, M. P., and J. Hallett, 1998: Ice crystal morphology in aircraft contrails and cirrus. Preprints, *14th Conf. on Cloud Physics,* Everett, WA, Amer. Meteor. Soc., 17–20.

——, P. J. DeMott, and W. R. Cotton, 1992: New primary ice-nucleation parameterization in an explicit model. *J. Appl. Meteor.,* **31,** 708–721.

Mitchell, D. L., 1988: Evolution of snow-size spectra in cyclonic storms. Part I: Snow growth by vapor deposition and aggregation. *J. Atmos. Sci.,* **45,** 3431–3451.

——, 1994: A model predicting the evolution of ice particle size spectra and radiative properties of cirrus clouds. Part I: Microphysics. *J. Atmos. Sci.,* **51,** 797–816.

Ohtake, T. K., 1993: Freezing point of H_2SO_4 aqueous solution and formation of stratospheric ice clouds. *Tellus,* **45B,** 138–144.

——, K. Jayaweera, and K.-I. Sakurai, 1982: Observation of ice crystal formation in lower Arctic atmosphere. *J. Atmos. Sci.,* **39,** 2898–2904.

Overland, J. E., and P. S. Guest, 1991: The Arctic snow and air temperature budget over sea ice during winter. *J. Geophys. Res.,* **96,** 4651–4662.

Pinto, J. O., 1998: Autumnal mixed-phase cloudy boundary layers in the Arctic. *J. Atmos. Sci.,* **55,** 2016–2038.

——, J. A. Curry, and C. W. Fairall, 1997: Radiative and microphysical properties of low-level Arctic clouds inferred from ground-based measurements. *J. Geophys. Res.,* **102,** 6941–6952.

Platt, C. M. R., and H. Harshvardhan, 1988: Temperature dependence of cirrus extinction: Implications for climate feedbacks. *J. Geophys. Res.,* **93** (D9), 11 051–11 058.

Pruppacher, H. R., and J. D. Klett, 1997: *Microphysics of Clouds and Precipitation.* 2d ed. Kluwer Academic Publishers, 955 pp.

Rangno, A. L., and P. V. Hobbs, 2001: Ice particles in stratiform clouds in the Arctic and possible mechanisms for the production of high ice concentrations. *J. Geophys. Res.,* in press.

Rogers, D. C., P. J. DeMott, and S. M. Kreidenweis, 2001: Measurements of ice nucleating aerosol particles in the Arctic. *J. Geophys. Res.,* in press.

Rogers, R. R., and M. K. Yau, 1989: *A Short Course in Cloud Physics.* 3d ed. Pergamon Press, 293 pp.

Rosinski, J., 1991: Latent ice forming nuclei in the Pacific Northwest. *Atmos. Res.,* **26,** 509–523.

——, C. T. Nagamoto, and M. Y. Zhow, 1995: Ice forming nuclei over the East China Sea. *Atmos. Res.,* **36,** 95–105.

Ruffieux, D., P. O. G. Persson, C. W. Fairall, and D. E. Wolfe, 1995: Ice pack and lead surface energy budgets during LEADEX 92. *J. Geophys. Res.,* **100,** 4583–4612.

Sassen, K., and G. C. Dodd, 1988: Homogeneous nucleation rate for highly supercooled cirrus cloud droplets. *J. Atmos. Sci.,* **45,** 1357–1369.

Schnell, R. C., 1984: Arctic haze and the Arctic Gas and Aerosol Sampling Program (AGASP). *Geophys. Res. Lett.,* **11,** 361–364.

Seinfeld, J. H., and S. N. Pandis, 1998: *Atmospheric Chemistry and Physics: From Air Pollution to Climate Change.* 1st ed. John Wiley and Sons, 1326 pp.

Shaw, G. E., 1983: On the aerosol particle size distribution spectrum in Alaskan air mass systems: Arctic haze and non-haze episodes. *J. Atmos. Sci.,* **40,** 1313–1320.

——, 1984: Microparticle size spectrum of Arctic haze. *Geophys. Res. Lett.,* **11,** 409–412.

——, 1986: Cloud condensation nuclei associated with Arctic haze. *Atmos. Environ.,* **20,** 1453–1456.

——, 1995: The Arctic haze phenomenon. *Bull. Amer. Meteor. Soc.,* **76,** 2403–2413.

Starr, D. O., and S. K. Cox, 1985: Cirrus clouds. Part I: A cirrus cloud model. *J. Atmos. Sci.,* **42,** 2663–2681.

Swanson, B. D., N. J. Bacon, E. J. Davis, and M. B. Baker, 1998: Levitated ice crystals: Laboratory measurements of ice particle breakup and growth/sublimation rate. Preprints, *14th Conf. on Cloud Physics,* Everett, WA, Amer. Meteor. Soc., 429–430.

Szyrmer, W., and I. Zawadzki, 1997: Biogenic and anthropogenic sources of ice-forming nuclei: A review. *Bull. Amer. Meteor. Soc.,* **78,** 209–228.

Thuman, W. C., and E. Robinson, 1954: Studies of Alaskan ice fog particles. *J. Meteor.,* **11,** 151–156.

Witte, H. J., 1968: Airborne observations of cloud particles and infrared flux density in the Arctic. Ph.D. thesis, University of Washington, 101 pp.